



1

2 Variability and long-term changes of brominated VSLS at the
3 tropical tropopause

4

5 **Susann Tegtmeier¹, Elliot Atlas², Birgit Quack¹, Franziska Ziska¹, and Kirstin Krüger³**

6

7

8 ¹GEOMAR Helmholtz Centre for Ocean Research Kiel, Kiel, Germany

9

10 ²Rosenstiel School of Marine and Atmospheric Science, University of Miami, Miami, Florida,
11 USA

12

13 ³Meteorology and Oceanography Section, Department of Geosciences, University of Oslo,
14 Oslo, Norway

15

16

17

18

19

20

21

22

23

24



1 Abstract

2

3 We combine available observational data sets with Lagrangian atmospheric modelling in order
4 to analyze the spatial and temporal variability of the CHBr_3 injection into the stratosphere.
5 Regional maxima with mixing ratios of up to 0.4-0.5 ppt at 17 km altitude are diagnosed to be
6 over Central America (1) and over the Maritime Continent/West Pacific (2), both of which are
7 confirmed by high-altitude aircraft campaigns. The CHBr_3 maximum over Central America is
8 caused by the co-occurrence of convectively-driven short transport time scales and strong
9 regional sources, which in conjunction drive the seasonality of CHBr_3 injection. Model results
10 at a daily resolution reveal isolated, exceptionally high CHBr_3 values in this region which are
11 confirmed by measurements during the ACCENT campaign and do not occur in spatially or
12 temporally averaged model fields. CHBr_3 injection over the West Pacific is centered south of
13 the equator due to strong oceanic sources underneath prescribed by the here applied bottom-up
14 emission inventory. The globally strongest stratospheric CHBr_3 injection of up to 0.6 ppt is
15 diagnosed to occur over the region of India, Bay of Bengal and Arabian Sea (3), however, no
16 data from aircraft campaigns are available to confirm this finding. Interannual variability of
17 stratospheric CHBr_3 injection of 10-20% is to a large part driven by the variability of coupled
18 ocean-atmosphere circulation systems. Long-term changes, on the other hand, correlate with
19 the regional SST trends resulting in positive trends of stratospheric CHBr_3 injection over the
20 West Pacific and Asian monsoon region and negative trends over the East Pacific. For the
21 tropical mean, these opposite regional trends balance each other out resulting in a relatively
22 weak positive trend of 0.017 ± 0.012 ppt Br/dec for 1979-2013, corresponding 3% Br/dec. The
23 overall contribution of CHBr_3 together with CH_2Br_2 to the stratospheric halogen loading
24 accounts for 4.7 ppt Br, in good agreement with existing studies, with 50%/50% being injected
25 in form of source and product gases, respectively.

26

27 1 Introduction

28

29 It has long been recognized that the depletion of stratospheric ozone over the last 30 years is
30 mainly caused by human-made chlorine- and bromine-containing substances, often referred to
31 as ozone-depleting substances (ODS) (Carpenter and Reimann et al., 2014). The Montreal



1 Protocol, crafted in 1987 to control the production and consumption of ODSs, has been very
2 successful in reducing the emission of the long-lived halocarbons. As a result, the overall
3 abundance of ODS in the atmosphere has been decreasing since the beginning of the 21st
4 century and the depletion of stratospheric ozone is expected to level off and reverse (Austin and
5 Butchart, 2003; Carpenter and Reimann et al., 2014).

6 In contrast to long-lived halocarbons, the so-called Very Short-Lived Substances (VSLS) with
7 chemical lifetimes of less than 6 months (e.g. Ko and Poulet et al., 2003), are not controlled by
8 the Montreal Protocol and are even suggested to increase in the future (e.g., Pyle et al., 2007;
9 Tegtmeier et al., 2015; Ziska et al., 2017). Brominated VSLS are primarily of natural origin
10 emitted by oceanic macroalgae and phytoplankton (e.g., Quack and Wallace, 2003). Over the
11 last years there has been increasing evidence from observational (e.g., Dorf et al., 2008; Sioris
12 et al., 2006; McLinden et al., 2010; Brinckmann et al., 2012) and modelling (e.g., Warwick et
13 al. 2006; Liang et al., 2010; Hossaini et al., 2012b; Tegtmeier et al., 2012) studies that VSLS
14 provide a significant contribution to stratospheric total bromine (Br_y). Current estimates of this
15 contribution range between 2 and 8 ppt (Carpenter and Reimann et al., 2014; Navarro et al.,
16 2015; Wales et al., 2018). The injection of VSLS into the stratosphere in form of source gases
17 (SGs) or inorganic product gases (PGs) depends strongly on the efficiency of troposphere-
18 stratosphere transport versus the degradation of the source gases (through photochemical loss)
19 and product gases (through wet deposition). In particular, the question of heterogeneous release
20 of bromine back to the gas phase, which determines the efficiency of wet deposition as a sink
21 for Br_y , is currently under discussion (Salawitch, 2006; Aschmann et al., 2011). Once
22 brominated VSLS have reached the stratosphere in the form of SG or PG, they participate in
23 ozone depletion at middle and high latitudes (Braesicke et al., 2013; Yang et al., 2014;
24 Sinnhuber and Meul, 2015). Through their relatively large impact on ozone in the lower
25 stratosphere, they contribute -0.02Wm^{-2} to global radiative forcing (Hossaini et al., 2015).

26 The most abundant bromine containing VSLS are bromoform (CHBr_3) and dibromomethane
27 (CH_2Br_2) and with potentially important source regions in tropical, subtropical and shelf waters
28 (e.g., Butler et al., 2007; Quack et al., 2007). The emissions of brominated VSLS from the
29 ocean into the atmosphere can be derived based on their concentration gradient between water
30 and air, wind speed, sea surface temperature and salinity (e.g. Nightingale et al. 2000; Quack
31 and Wallace 2003; Ziska et al. 2013). The magnitude and distribution of brominated VSLS
32 emissions are poorly constrained given the sparse observational data base of their oceanic and



1 atmospheric concentrations (Ziska et al., 2013). Current emission inventories have been mostly
2 derived via the top-down approach by adjusting the estimated VSLs emissions in a global
3 atmospheric model to produce agreement of the model simulations with aircraft observations.
4 For CHBr_3 , the current global top-down emissions range between 426 - 530 Gg Br/year (Liang
5 et al., 2010; Warwick et al., 2006, Ordonez et al., 2012), while the bottom-up approach based
6 on statistical gap filling of an observational data base suggests smaller global fluxes of 164-236
7 Gg Br/year (Ziska et al., 2013). A recent oceanic modelling study taking into account source
8 and sink processes projects open ocean emissions of around 72 Gg Br/year in form of CHBr_3 ,
9 not including the strong coastal sources (Stemmler et al., 2015). Quantitative evaluations of
10 various emission inventories demonstrated that the performance of the individual inventories
11 depends strongly on the region and model applied for the evaluation (Hossaini et al., 2013;
12 Hossaini et al., 2016).

13 Stratospheric injection of trace gases with lifetimes of days to weeks is most efficient in regions
14 of strong, high reaching convective activity such as the West Pacific (e.g., Aschmann et al.,
15 2009; Pisso et al., 2010; Marandino et al., 2013). The Asian monsoon represents another
16 important pathway to the lower stratosphere (e.g., Randel et al. 2010, Tissier and Legras, 2016)
17 entraining mostly Southeast Asian planetary boundary layer air with the potential to include
18 emissions from the Indian Ocean and Bay of Bengal (Fiehn et al., 2017, 2018). In both regions,
19 the West Pacific and the Indian Ocean, these effective transport pathways may coincide with
20 strong oceanic emissions (e.g., Ziska et al., 2013) potentially leading to anomalously large
21 injection of brominated VSLs. While aircraft measurements in the West Pacific have confirmed
22 high concentrations of brominated VSLs such as CHBr_3 (Wales et al., 2018), the role of the
23 Asian monsoon as an entrainment mechanism for VSLs is not clear due to the lack of
24 observations in this region. Given the high variability of VSLs measurements in the tropical
25 tropopause layer (TTL) (Liang et al., 2010), the overall distribution and temporal short- and
26 long-term changes are not well known. Modelling the VSLs distribution in this region depends
27 on the magnitude and distribution of prescribed oceanic emissions, on the representation of
28 tracer transport in the models and on related uncertainties in both quantities (Hossaini et al.,
29 2016). Reconciling snapshots of VSLs distributions derived from high resolution aircraft
30 measurements with lower spatially and temporally smoothed global modelling fields remains a
31 challenge.



1 Changes in oceanic biogeochemical systems over the last decades most likely lead to changes in
2 the marine VSLs production. However, due to the sparse data coverage and missing process
3 understanding, it is currently not possible to quantify such long-term changes of the oceanic
4 halocarbon production and consequences for the air-sea flux (Ziska et al., 2017). Changes in
5 meteorological and oceanic surface parameters, which also impact the oceanic emission strength,
6 on the other hand, have been quantified. Based on increasing sea surface temperature, salinity
7 and wind speed, VSLs emissions are projected to increase over the recent past (Ziska et al.,
8 2013) and for future climate projections until 2100 (Tegtmeier et al., 2015, Ziska et al., 2017).
9 At the same time, atmospheric transport of VSLs is driven by changes of the atmospheric
10 circulation. In particular, changes of tropical, high reaching convection can be expected to have
11 a large influence on the transport of VSLs from the ocean surface to the TTL (Aschmann et al.,
12 2011; Hossaini et al., 2013). Long-term changes of VSLs injections into the stratosphere are
13 difficult to predict as they are driven by various processes including changes in surface
14 emissions, troposphere-stratosphere transport, and tropospheric chemistry (Pyle et al., 2007;
15 Hossaini et al., 2012a).

16 In our study, we combine available observational data sets, including surface and upper air
17 measurements, with high resolution atmospheric modelling in order to analyze the spatial and
18 temporal variability of VSLs injection into the stratosphere. Model simulations and data sets
19 are introduced in Section 2. A detailed picture of the distribution of CHBr_3 in the TTL (Section
20 3.1) is derived from Lagrangian transport simulations applied to a bottom-up, observation-
21 based emission inventory. Analyses of the trajectory pathways and comparisons to aircraft
22 observations allow us to evaluate how well we know the hotspots of CHBr_3 injection (Sections
23 3.2 to 3.4). The question if such hotspots are mainly driven by oceanic or by atmospheric
24 processes will be answered based on the Lagrangian simulations. We present the first estimates
25 of the long-term changes of CHBr_3 injection based on changing oceanic emissions and transport
26 processes (Section 3.5). Finally, the overall contribution of CH_2Br_2 and CHBr_3 to the
27 stratospheric bromine loading is determined from the model simulations (Section 3.6) and
28 compared to existing studies. A summary and discussion of the key results is given in Section
29 4.

30



1 **2 Data and Model**

2 **2.1 Global emission climatology**

3 The global emission scenario from Ziska et al. (2013) is a bottom-up estimate of oceanic CHBr_3 ,
4 CH_2Br_2 , and CH_3I fluxes. Here we focus on the two brominated compounds. Global surface
5 concentration maps of the two compounds were generated from atmospheric and oceanic
6 surface ship-borne in-situ measurements collected within the HalOcAt (Halocarbons in the
7 ocean and atmosphere) database project (<https://halocat.geomar.de>). In a first step, the in-situ
8 surface measurements were classified based on physical and biogeochemical characteristics of
9 the ocean and atmosphere important for the CH_2Br_2 and CHBr_3 distribution and sources. In a
10 second step, the global $1^\circ \times 1^\circ$ grid was filled by extrapolating the in-situ measurements within
11 each classified region based on the ordinary least square and robust fit regression techniques.
12 The method includes all in situ-measurements available through the HalOcAt data base at the
13 time, regardless of season and year of the measurement. The resulting concentration maps are
14 taken to represent climatological fields of a 23 year long time period covering 1989 to 2011.
15 Based on the global concentration maps the oceanic emissions were calculated with the transfer
16 coefficient parameterization of Nightingale et al. (2000), which was adapted to CHBr_3 and
17 CH_2Br_2 (Quack and Wallace, 2003). While the concentration maps do not provide any temporal
18 variability, the emission parameterization is based on 6 hourly meteorological ERA-Interim
19 data (Dee et al., 2011) allowing for relative emission peaks related to maxima in the horizontal
20 wind fields and sea surface temperature. The emission inventory is available at 6-hourly, daily,
21 and monthly temporal resolution or as a climatology product calculated as a long-term average
22 emission field.

23 **2.2 Aircraft campaigns**

24 We analyze the spatial and temporal variability of CHBr_3 in the TTL based on the comparison
25 of Lagrangian transport simulations to data from aircraft campaigns. CHBr_3 measurements in
26 the upper TTL are currently available from seven aircraft campaigns. Nearly all of the
27 campaigns took place over Central America, except for the ATTREX campaign which was in
28 large part conducted over the Pacific. Detailed information about the aircraft missions including
29 location and time period are presented in Table 1.

30



1 **Table 1.** Aircraft campaigns with CHBr_3 measurements used in the study.

Campaign (Aircraft)	Full name	Max. altitude	Location	Time period	Database/ Reference
ACCENT (WB-57)	Atmospheric Chemistry of Combustion Emissions Near the Tropopause	19 km	Southern US Gulf of Mexico East Pacific	1999 April, September	http://espoarchive.nasa.gov/archive/browse/accent
Pre-AVE (WB-57)	Pre-Aura Validation Experiment	19 km	Southern US Gulf of Mexico East Pacific	2004 January – February	http://espoarchive.nasa.gov/archive/browse/pre_ave
AVE (WB-57)	Aura Validation Experiment	19 km	Southern US Gulf of Mexico	2005 June	https://espoarchive.nasa.gov/archive/browse/ave
CR-AVE (WB-57)	Aura Validation Experiment (Costa Rica)	19 km	Southern US Gulf of Mexico East Pacific	2006 January - February	https://espoarchive.nasa.gov/archive/browse/cr_ave
TC4 (WB-57)	Tropical Composition, Cloud and Climate Coupling	19 km	Southern US Gulf of Mexico East Pacific	2007 August	Toon et al. (2010)
SEAC4RS (ER-2)	Studies of Emissions, Atmospheric Composition, Clouds and Climate Coupling by Regional Surveys	19 km	Southern US Gulf of Mexico	2013 September	https://espo.nasa.gov/missions/seac4rs
ATTREX (Global Hawk)	Airborne Tropical Tropopause Experiment	19 km	East Pacific	2013 February - March	http://espo.nasa.gov/missions/attrex
		18 km	West Pacific	2014 February - March	

2



1 2.3 VLSL transport modeling

2

3 We are interested in the direct contribution of CHBr_3 and CH_2Br_2 to stratospheric halogen
4 loading in the form of source and product gas contributions. Therefore, the atmospheric
5 transport of the two compounds from the oceanic surface into the upper troposphere and TTL
6 is simulated with the Lagrangian particle dispersion model FLEXPART (Stohl et al., 2005)
7 Version 9.2 beta. The oceanic emissions, based on the sea-to-air flux data from Ziska et al.
8 (2013), prescribe the amount of CH_2Br_2 and CHBr_3 released in the FLEXPART simulations
9 with each air parcel trajectory. The global sea-to-air flux, given on a $1^\circ \times 1^\circ$ grid, is used here at
10 a monthly mean temporal resolution. For CHBr_3 , 90 trajectories are released per month from
11 each grid box carrying the gas amount prescribed by the emission scenario. For the longer-lived
12 CH_2Br_2 , 45 trajectories are released per month. Once all brominated SG and PG has been
13 removed from a trajectory through chemical decay and wet deposition, the trajectory is
14 automatically terminated, so that the number of all active trajectories stays roughly constant (~
15 20 million) at all times after the initial spin-up period. The global CHBr_3 simulations are run
16 for 35 years from 1979 to 2013 with a spin-up period of 6 months, while the CH_2Br_2 runs are
17 carried out for three years from 2011 to 2013 with a spin-up period of 18 months.

18 The transport in FLEXPART is driven by meteorological fields from the ECMWF (European
19 Centre for Medium-Range Weather Forecasts) reanalysis model. FLEXPART includes
20 parameterizations for moist convection (Forster et al., 2007) and turbulence in the boundary
21 layer and free troposphere (Stohl and Thomson, 1999), dry deposition, and scavenging (Stohl
22 et al., 2005). The runs are based on the 6-hourly fields of horizontal and vertical wind,
23 temperature, specific humidity, convective precipitation, and large scale precipitation from the
24 ECMWF reanalysis product ERA-Interim (Dee et al., 2011) given at a horizontal resolution of
25 $1^\circ \times 1^\circ$ on 60 model levels. A pre-processor retrieves the meteorological fields from the ECMWF
26 archive, including the vertical wind, which is calculated in hybrid coordinates mass-consistently
27 from spectral data. FLEXPART has been validated based on comparisons with measurement
28 data from three large-scale tracer experiments (Stohl et al., 1998) and with results from
29 intercontinental air pollution transport studies (e.g., Forster et al., 2001; Stohl and Trickl, 1999).
30 Previous FLEXPART studies using a similar model setup as applied here have shown a very
31 good agreement between diagnosed and observed VLSL profiles (e.g., Tegtmeier et al., 2013;
32 Fuhlbrügge et al., 2016).



1 FLEXPART includes the simulation of chemical decay by reducing the tracer mass carried by
2 each air parcel corresponding to its prescribed chemical lifetime. We set the atmospheric
3 lifetime of CHBr_3 (CH_2Br_2) to an altitude-dependent lifetime profile ranging from 16 (50) days
4 at the ocean surface to 29 (400) days in the TTL (Hossaini et al., 2012b). The lifetime profiles
5 were derived from simulations of the chemical tropospheric loss processes of CHBr_3 and
6 CH_2Br_2 with the chemical transport model TOMCAT (Chipperfield, 2006). Previously, profiles
7 from TOMCAT have been shown to agree well with aircraft observations in the tropical
8 troposphere (Hossaini et al., 2012b).

9 The bromine resulting from the photochemical loss of CH_2Br_2 and CHBr_3 contributes to the
10 inorganic product gases. In the FLEXPART simulations, these product gases are grouped
11 together as Br_y and transported together with the VSLS source gases along the trajectory. Br_y
12 can be removed effectively from the troposphere through wet scavenging by rain or ice (Yang
13 et al., 2005). FLEXPART includes in-cloud as well as below-cloud scavenging, which is
14 initiated if the relative humidity as calculated from meteorological input data exceeds 80% and
15 the precipitation rate is larger than zero. The wash-out of the soluble inorganic bromine species
16 HOBr and HBr is modeled via the cloud scavenging ratio calculated using the effective Henry's
17 Law coefficient. In order to determine which fractions of Br_y are in the form of HBr and HOBr ,
18 we apply the Br_y partitioning derived from p-TOMCAT simulations (Yang et al., 2010) as
19 described in detail by Tegtmeier et al. (2012). Note that the chemical scheme of p-TOMCAT
20 includes heterogeneous reactions on aerosols which reactivate bromine radicals from the
21 reservoir species (Yang et al., 2005; 2010). By directly using the p-TOMCAT Br_y partitioning
22 in the FLEXPART model runs these aerosol effects have been taken into consideration when
23 simulating the wet removal of Br_y .

24 For the analysis of the spatial and temporal variability of CHBr_3 in the TTL from FLEXPART
25 simulations and aircraft observations in Sections 3.1 to 3.5, we use mixing ratios at 17 km
26 (approximate cold point) and mixing ratios averaged over 16-18 km (upper part of the TTL). In
27 order to derive the amount of VSLS source and product gases entrained into the stratosphere
28 from the model simulations in Section 3.6, we explicitly calculate the cold point along each
29 trajectory as stratospheric entrainment point. The derived estimates of stratospheric VSLS
30 entrainment depend on the meteorological input data sets and on various FLEXPART model
31 parameters, such as the convective parameterization. The accurate representation of convection
32 has been validated with tracer experiments and ^{222}Rn measurements (Forster et al., 2007). The



1 application of transport timescales based on vertical heating rates instead of vertical wind fields
2 in the TTL between 15 and 17 km results in only minor differences of VSLs entrainment
3 (Tegtmeier et al., 2012). Uncertainties in the modeled wet deposition can, among others, arise
4 from uncertainties in the Br_y partitioning prescribed by p-TOMCAT related to uncertainties in
5 the aerosols loading and in the mechanism used for heterogeneous reactions.
6



1 **3 Results**

2

3 **3.1 CHBr₃ in the TTL**

4

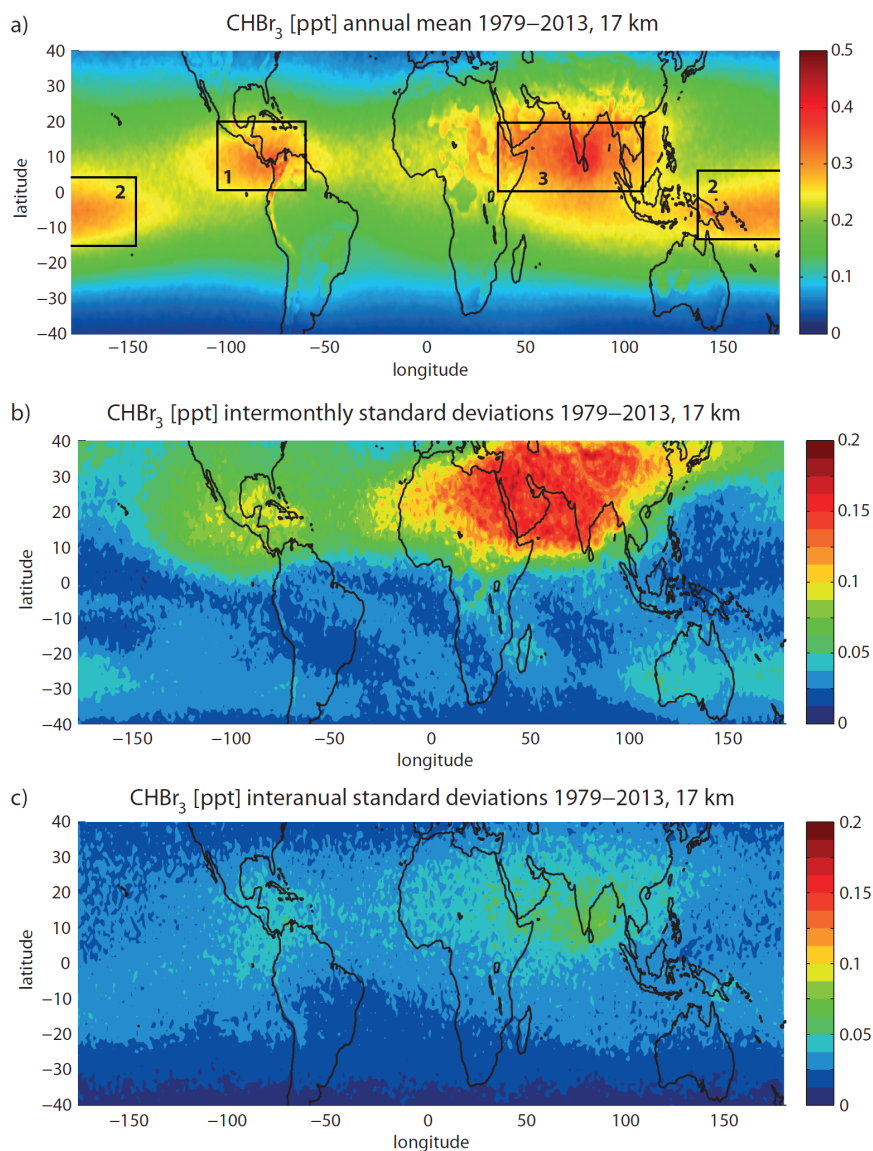
5 Figure 1a shows the long-term annual mean CHBr₃ distribution at 17 km as derived from the
6 Lagrangian transport calculations driven by monthly mean oceanic emission fields for the time
7 period 1979 – 2013. Clearly, CHBr₃ has a very pronounced spatial variability due to its short
8 lifetime. Largest CHBr₃ mixing ratios of up to 0.4 to 0.5 ppt can be found over 1) Central
9 America, 2) the maritime continent and tropical West Pacific and 3) tropical Indian Ocean (all
10 regions are highlighted by black squares in Figure 1a labelled from 1 to 3). Other tropical
11 regions with only little convective uplift show smaller mixing ratios, mostly between 0.1 and
12 0.2 ppt.

13 Entrainment of CHBr₃ into the stratosphere shows also a large temporal variability. The
14 seasonal variability is given here by the standard deviation over all monthly, multi-annual mean
15 values (Figure 1b). The by far most pronounced variability is found in the region of the Asian
16 Monsoon anticyclone, which is characterized by a strong seasonality of vertical transport
17 processes (Randel et al., 2010). Furthermore, the distribution of CHBr₃ at the cold point over
18 Central America shows some seasonal variations; however, of smaller magnitude. The maritime
19 continent and tropical West Pacific have only a very weak seasonal cycle. Overall, the seasonal
20 variations are more pronounced in the NH tropics and quite low in the SH tropics. Interannual
21 variations are given in form of the standard deviation over all annual mean CHBr₃ mixing ratios
22 at 17 km (Figure 1c). In comparison to the seasonal variability, the interannual variability is
23 relatively small in the NH tropics, but is of similar magnitude in the SH tropics. Drivers of the
24 seasonal and interannual variability will be discussed in the following sections.

25 In the following, we will analyze the three regions with maximum CHBr₃ entrainment identified
26 above, and investigate the relative importance of emissions and transport processes for the
27 overall distribution and seasonality of stratospheric injection.

28

29



1
2
3
4
5
6
7

Figure 1. Modeled annual mean distribution of CHBr_3 at 17 km for 1979–2013 (a) and the inter-monthly (b) and inter-annual (c) variations given by the standard deviations over all monthly, multi-annual mean and annual mean values, respectively.



1 3.2 Central America

2

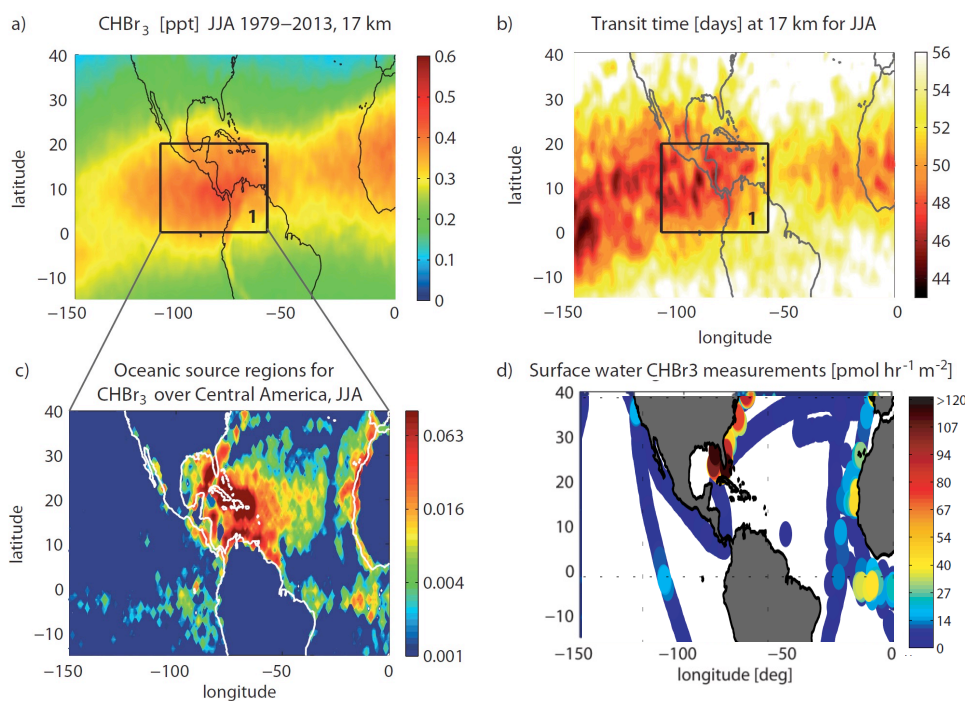
3 CHBr₃ in the TTL, on its way from the ocean surface to the stratosphere, shows a pronounced
4 maximum over Central America between 0°-20°N and 60°W-110°W (black square in Figures
5 1a and 2a). This maximum is present all year, but most pronounced during NH summer and
6 autumn. In the following, we will use the simulations for June/July/August to address the
7 question, if this maximum arises from very strong oceanic sources or from strong convective
8 transport. The impact of transport on the CHBr₃ distribution in the upper TTL is analyzed by
9 estimating the time air masses need from the ocean surface to 17 km based on the FLEXPART
10 model simulations. The transport time of each trajectory is assigned to the location where the
11 trajectory reaches 17 km. A map of the ‘ocean surface – 17 km transit times’ is derived by
12 averaging over all trajectories on a 1°x1° grid. The tropical annual mean transit time is around
13 55 days with variations between 45 and 70 days (not shown here). Transit times over Central
14 America for the June/July/August season are relatively short with values around 48 days (Figure
15 2b). However, the transit times over the East and Central Pacific are similar or even shorter,
16 suggesting that the vertical transport in this region is as efficient as over Central America.
17 Therefore, atmospheric transport time scales alone cannot explain the CHBr₃ maximum over
18 Central America.

19 In addition to the transit time, we analyze the oceanic sources of CHBr₃ over Central America.
20 Each trajectory reaching the TTL over Central America (black square in Figure 2a) contributes
21 a certain amount of CHBr₃ to this local maximum by carrying its prescribed oceanic emission
22 (Ziska et al., 2013) from the surface to the cold point. The relative contribution (in %) of each
23 trajectory is assigned to its oceanic release point, thus quantifying which ocean region
24 contributes the largest amounts of CHBr₃ to the local maximum in the TTL. The relative
25 contributions averaged over 1°x1° grid cells (Figure 1c) demonstrate that the largest sources
26 stem from the Gulf of Mexico, the Caribbean Sea and the western North Atlantic. Some smaller
27 contributions come from the west coast of North Africa and from the equatorial Atlantic. The
28 co-occurrence of strong sources and the relatively short transport time scales over the Caribbean
29 Sea and Central America mainly cause the local CHBr₃ maximum in the Central American
30 TTL. While transport time scales are also short (or even shorter) in the eastern Pacific, oceanic
31 emissions are very small there and vice versa more pronounced emissions over the Atlantic and
32 along the coast of Africa do not cause a global maximum due to longer transport time scales.



1 The regional oceanic measurements in surface water, which were used to derive the
2 extrapolated concentration and emission maps (Ziska et al., 2013), are given in Figure 2d. The
3 available data show in particular high oceanic CHBr_3 concentrations at the Florida coastline
4 and in the eastern part of the Gulf of Mexico. A reasonable amount of measurements with a
5 distinctive distribution is available in this region supporting the extrapolated climatological
6 source distribution, which leads to the CHBr_3 maximum in the TTL over Central America
7 discussed above.

8



9

10 **Figure 2.** Modeled distribution of CHBr_3 at 17 km for JJA, 1979-2013 (a), transit time of air masses
11 from the ocean surface to the TTL (b), oceanic source regions for CHBr_3 over Central America at 17
12 km given in percent per $1^\circ \times 1^\circ$ grid box (c), and measurements of oceanic CHBr_3 concentrations from
13 the HalOcAt database used for Ziska et al. (2013) (d).

14

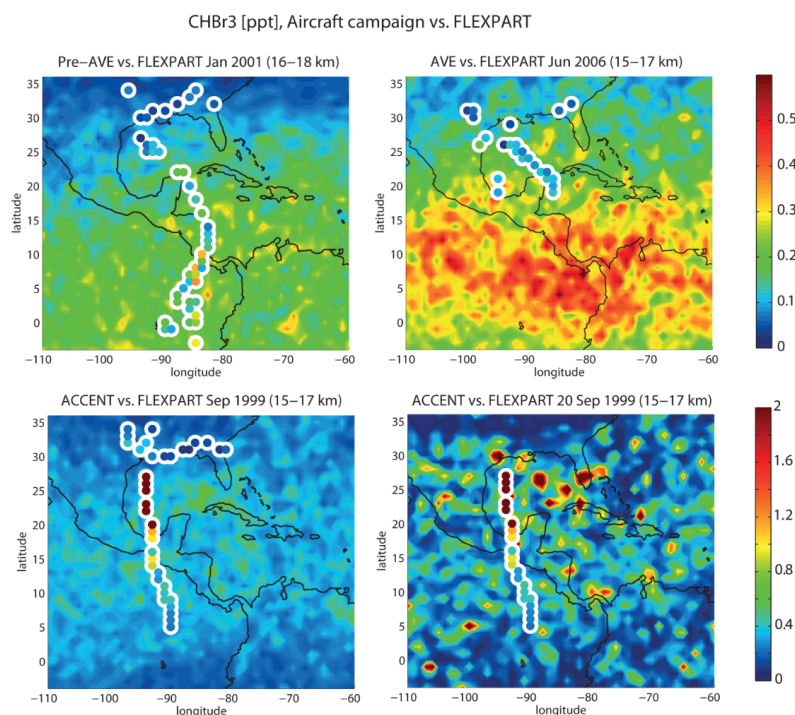
15 Over the last decades, the atmospheric distribution of CHBr_3 over Central America has been
16 investigated by a number of different aircraft campaigns. We will use available upper air



1 measurements to evaluate the distribution and variability of the model-derived CHBr_3 fields.
2 Details of the aircraft campaigns are given in Table 1. We show the spatial CHBr_3 distribution
3 in the TTL as observed during three different campaigns in comparison to the model simulations
4 (Figure 3). The altitude ranges in the upper TTL have been chosen so that each comparison
5 includes a maximum number of observational data. While for the aircraft campaigns individual
6 measurements are shown at the measurement locations, the model fields are averaged over the
7 duration of the respective campaign. This method allows us to evaluate the spatial distribution
8 of measured and modeled CHBr_3 fields, but it has the disadvantage of comparing in-situ data
9 with temporally averaged fields. We will discuss how this can impact the comparison and how
10 the temporal variability can be taken into account.

11 For the Pre-AVE campaign during Northern Hemisphere (NH) winter, CHBr_3 in the upper TTL
12 (16-18 km) shows a latitudinal gradient with small values of 0-0.1 ppt in the northern subtropics
13 and with higher values of up to 0.3-0.4 ppt around the equator. The same gradient is also evident
14 from the model simulation resulting in an overall good agreement. Similarly, for the AVE
15 campaign during NH summer, both, the observations and the model results, show a latitudinal
16 gradient with increasing values towards lower latitudes. However, here the overall agreement
17 is poor, since the model results are on average 50% larger than the measurements.

18



1

2 **Figure 3.** Modeled distribution of CHBr₃ in the upper TTL from FLEXPART (background coloring) in
3 comparison with aircraft campaign measurements (colored symbols with white edges). In the upper
4 panels and lower left panel, all individual measurements from the respective campaign and the model
5 mean over the same time period are shown. Only in the lower right panel, one individual flight
6 (ACCENT flight from 20.09.1999) is shown with FLEXPART daily mean values to illustrate the large
7 spatial variability including maximum values ≥ 2 ppt.

8

9 Finally, for the ACCENT campaign during NH autumn, the observations reveal extremely high
10 CHBr₃ (up to 2 ppt) between 30°N and 20°N. While CHBr₃ is decreasing north and south of
11 this area towards the range of 0.5-1 ppt, the values are still very high when compared to other
12 campaigns over Central America. FLEXPART results, averaged over the time period of the
13 ACCENT campaign (Sep 1999), show largest monthly mean CHBr₃ values of around 0.7 ppt,
14 which are substantially smaller than the observations of 2 ppt. However, the model results look
15 quite different and show large spatial inhomogeneities when evaluated at a daily mean
16 resolution. Maximum model values are much higher for the daily resolution and in some
17 locations, very close to the flight track, of similar size as the observations (around 2 ppt). The



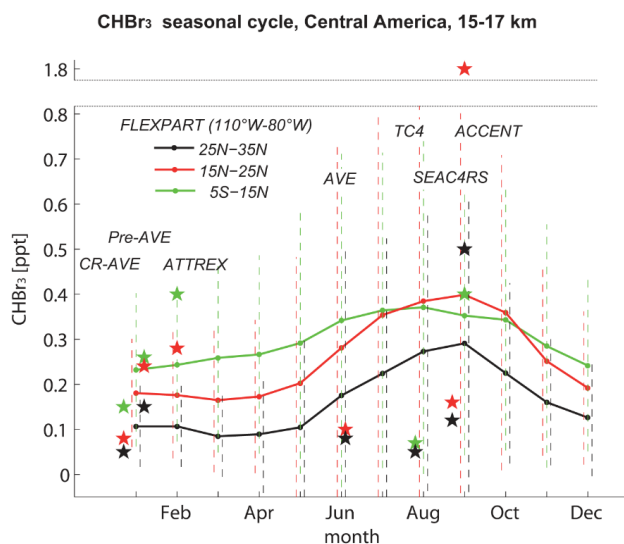
1 differences between monthly and daily mean model values make clear that CHBr_3 model-
2 measurement comparisons may be obscured by the high variability of the field. Given this high
3 variability and the existing uncertainties in the diagnosed oceanic sources and atmospheric
4 transport processes, it is very difficult for a model to predict the correct in-situ values at a given
5 time and measurement position. Nevertheless, if the large-scale emissions and transport fields
6 are correct, spatial and temporal averaging of the model results can be expected to produce
7 realistic mean VSLS fields and to improve the agreement with observations. Only in cases
8 where rare events have been observed, averaging the CHBr_3 fields will not necessarily lead to
9 a better agreement with the measurements, as demonstrated above for the ACCENT campaign.
10 In consequence, it is important to include estimates of the spatial and temporal variability of
11 the CHBr_3 field in all comparisons.

12 A summary of CHBr_3 model results compared to all aircraft campaigns in the Central American
13 region, taking into account above discussed spatial and temporal variability, is provided in
14 Figure 4. Here, we compare averages calculated over different parts of the flight tracks (split
15 by latitude) with FLEXPART results averaged over the same latitudinal bin and over 110°W -
16 80°W , the main longitudinal extent of the aircraft campaigns. While the campaign results refer
17 to the respective individual years (given in Table 1), FLEXPART results are averaged over the
18 entire campaign time period (1999-2013). In order to account for the fact that the model results
19 are averaged over space and time, the variability of the simulated CHBr_3 distribution is given
20 by the standard deviation over all daily mean values in the respective region. The comparison
21 of the three campaigns during NH winter shows an overall good agreement. For some latitude
22 bins, the modelled mean values agree very well with the observations (e.g., Pre-AVE for 5°S -
23 15°N), for other regions, differences of the mean values can be up to 50-100%. However, all
24 observational mean values are within the standard deviations of the modelled field indicating
25 good agreement of model and measurements.

26

27

28



1

2 **Figure 4.** Seasonal cycle of CHBr_3 in the upper TTL (15-17 km) over Central America from
3 FLEXPART simulations (dots and solid lines) in comparison with aircraft campaign measurements
4 (stars). FLEXPART results are averaged over 110°W-80°W and 5°S-15°N (green), 15°N-25°N (red),
5 and 25°N-35°N (black). Aircraft measurements are averaged over the same latitude bins and correspond
6 to the respective year of the campaign. The FLEXPART seasonal cycle is taken over the time period
7 1999 to 2013. Temporal and spatial variability is shown in form of the 1-sigma standard deviations over
8 all values in the respective bin and time period as dashed vertical lines.

9

10 For the campaigns during NH summer, mean differences are larger in most cases. At the same
11 time, the temporal and spatial variability of the simulated CHBr_3 distribution is also larger so
12 that nearly all observations fall within the simulated uncertainty. The large differences between
13 the individual campaigns during NH summer confirm the increased variability suggested by the
14 model results. For three of the campaigns, FLEXPART overestimates the CHBr_3 values during
15 this time of the year, while for the last campaign (ACCENT), the modelled mean values are
16 smaller. Particularly high CHBr_3 exists for the 15°N-25°N region, observed during the
17 ACCENT campaign at the top altitude of a plume extending from 14 – 16 km near Houston,
18 Texas. This value is larger than the model mean and also outside of the given variability range.
19 As discussed earlier, the model results also include such high values on a daily mean basis, but
20 only in rare occasions, suggesting that during the ACCENT campaign extraordinary
21 atmospheric conditions with very effective convection were observed.

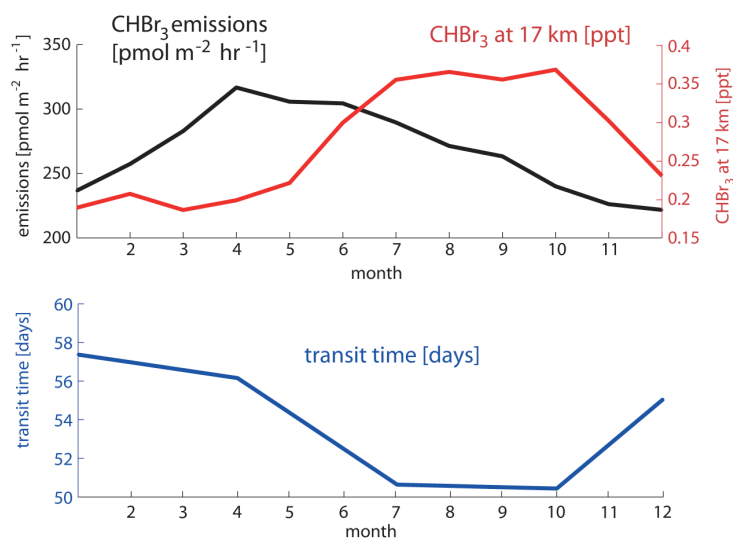


1

2 CHBr₃ in the upper TTL over Central America shows pronounced seasonal variations as
3 revealed by the comparisons to aircraft campaigns in Figure 4. The CHBr₃ seasonal cycle at 17
4 km shows a maximum from July to October (~0.37 ppt) and a minimum from January to April
5 (~0.17 ppt) (Figure 5a). Such seasonal variations can be caused by variations of the oceanic
6 emissions or the atmospheric transport times. First, we analyze the seasonal cycle of CHBr₃
7 emissions, averaged over the source region identified earlier, which show peak emissions from
8 April to June of up to 320 pmol m⁻² hr⁻¹. This peak in surface emissions in late spring/early
9 summer is consistent with a peak in the TTL around 2 months later, as the mean transit time
10 from the surface to 17 km in this region is about 55 days. Second, we analyze the seasonal cycle
11 of the transit time and find a minimum from July to October, which is also consistent with the
12 highest CHBr₃ values in the TTL during the same time period. While the amplitude of the
13 seasonal cycle in CHBr₃ in the TTL is around 74%, seasonal variation of the emissions and the
14 transit time are only 36% and 15%, respectively. However, the amplitude in transit time does
15 not directly translate into the amplitude in CHBr₃ in the TTL, given the logarithmic nature of
16 the atmospheric lifetime of chemical compounds. Overall, the interaction of both processes,
17 oceanic emissions and transit time, cause the pronounced seasonal cycle of CHBr₃ over Central
18 America.

19

20



1

- 2 **Figure 5.** Seasonal cycle of CHBr₃ at 17 km over Central America (black square in Figure 2a) from
3 FLEXPART simulations (red line), of oceanic CHBr₃ emissions averaged over the respective source
4 region (black line) and of the ‘surface – 17 km’ mean transit time (blue line) are shown.



1 **3.3 Maritime Continent and tropical West Pacific**

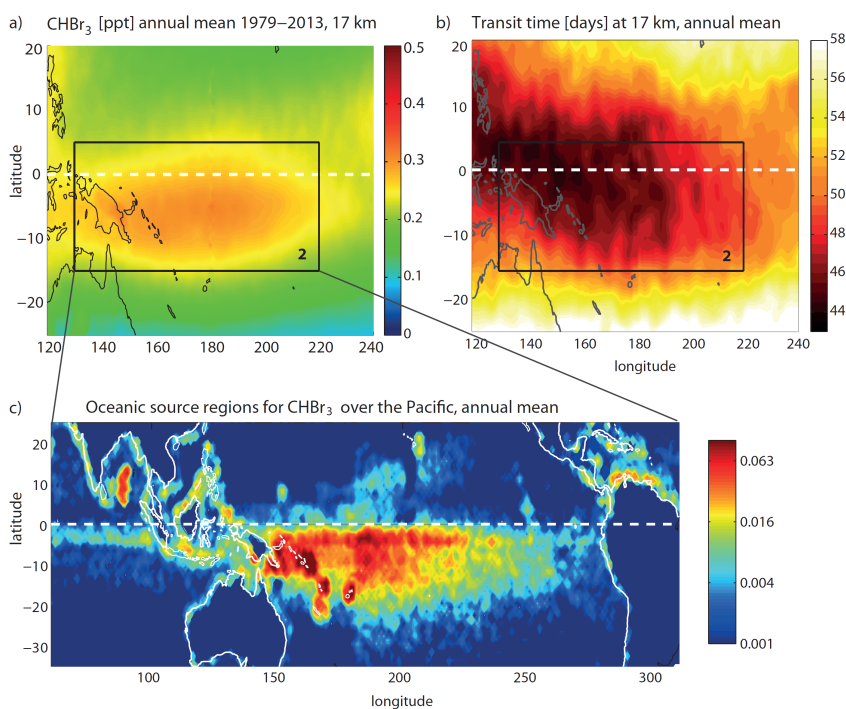
2

3 CHBr₃ in the TTL shows a pronounced maximum over the Maritime Continent and tropical
4 West Pacific between 15°S-5°N and 130°E-220°E (black square in Figures 1a and 6a). An
5 important characteristic of this CHBr₃ maximum (referred to as the West Pacific maximum
6 hereinafter) is that the high values are not distributed symmetrically across the equator, but are
7 shifted southwards. The maximum is present all year with no pronounced seasonal cycle (see
8 Figure 1b). In the following, we will use annual mean results to investigate if the high values
9 arise from very strong oceanic sources or from strong convective transport. The transit time
10 shows smallest values of around 45 days in the West Pacific and over the Maritime continent
11 (Figure 6b). The most important deviation from the CHBr₃ distribution at 17 km is that over the
12 West Pacific the shortest time scales and thus most efficient transport are not centered in the
13 Southern Hemisphere, but they are distributed symmetrically across the equator.

14 Oceanic sources for CHBr₃ in the West Pacific upper TTL (black square in Figure 6a) stem
15 mostly from the Pacific Ocean, the Maritime Continent and also to a smaller degree from
16 Central America (Figure 6c). The trajectory analysis clearly shows that the largest contribution
17 comes from the West Pacific south of the equator, while the oceanic contributions north of the
18 equator are lower. This pattern is directly related to the emission inventory used in this study
19 (Ziska et al., 2013), which suggests overall stronger emissions in the southern Pacific Ocean.
20 However, available open ocean surface measurements in both, NH and SH Pacific Ocean, were
21 sparse during the time of the construction of the inventory and mostly based on the TransBrom
22 Sonne campaign (Krüger and Quack, 2013). The latitudinal gradient of the emission inventory
23 with stronger emissions in the SH is based on the in-situ measurements along one cruise track
24 from Japan to Australia during October 2009 and may not be representative for other seasons
25 and other West Pacific regions. Future ship campaigns are necessary to confirm or improve the
26 existing emission inventory.

27

28



1

2 **Figure 6.** Modeled distribution of CHBr₃ at 17 km, annual mean 1979-2013 (a), transit time of air
3 masses from the ocean surface to the TTL (b), oceanic source regions for West Pacific CHBr₃ at 17 km
4 given in percent per 1°x1° grid box (c).

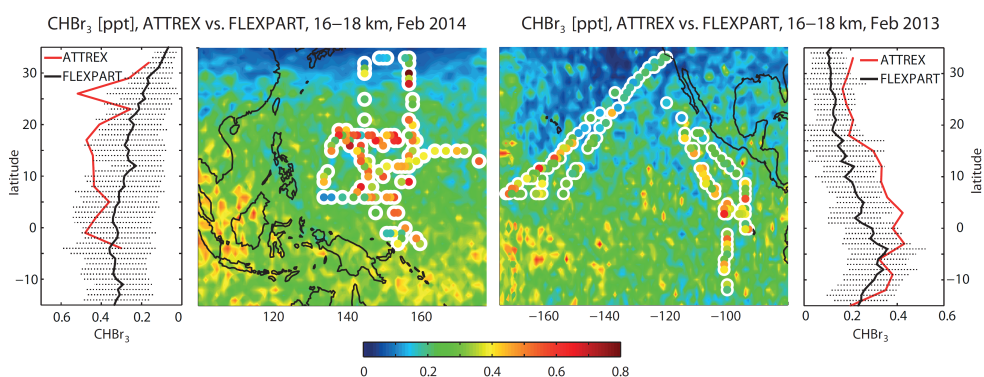
5

6 Pacific aircraft campaigns are used to further analyze the hemispheric differences of the
7 diagnosed CHBr₃ distribution. ATTREX measurements in the West Pacific in 2014 and in the
8 East Pacific in 2013 are compared to FLEXPART simulations in Figure 7. In both regions, the
9 comparison reveals a reasonably good agreement with increasing CHBr₃ values towards lower
10 latitudes. Observations and model results agree well north of 20°N with mean values around
11 0.2-0.3 ppt CHBr₃, except for one outlier in the West Pacific between 25°N and 30°N. During
12 this event, extraordinary high CHBr₃ values have been observed leading to a spike in the zonal
13 ATTREX profile which is not reproduced by the model simulations. South of the equator,
14 observations and model results also show a good agreement with relatively small differences
15 of up to 25%. Between 0-20°N, however, substantial differences are found. The model results
16 (0.2 – 0.3 pptv) clearly underestimate the observations (0.4 – 0.6 pptv) and cause differences
17 up to 100%, at some latitudes exceeding the uncertainty range (dashed horizontal lines) given



1 by the spatial and temporal variability of the bromoform distribution. The disagreement
2 between model simulations and observations at these latitudes suggests, that the emissions
3 gradient across the equator may not be a realistic phenomenon throughout the year and that
4 larger emissions and thus also larger TTL values can be expected north of the equator.

5



6

7

8 **Figure 7.** Modeled distribution of CHBr₃ in the uppermost TTL from FLEXPART (background
9 coloring) in comparison with ATTREX aircraft campaign measurements (colored symbols with white
10 edges). Zonal mean comparisons are given in the leftmost panel for FLEXPART and the ATTREX
11 campaign in February/March 2014 in the West Pacific and in the rightmost panel for FLEXPART and
12 the ATTREX campaign in February/March 2013 in the East Pacific.



1 3.4 Tropical Indian Ocean

2

3 Annual mean CHBr_3 in the uppermost TTL shows a pronounced maximum over India, the Bay
4 of Bengal and the Arabian Sea between 2°N - 22°N and 35°E - 110°E (Figures 1a, referred to as
5 the Indian Ocean maximum hereinafter). The simulations diagnose in the long-term mean, the
6 globally highest TTL CHBr_3 values of up to 0.5 ppt over the southern tip of India. At the same
7 time, the intermonthly standard deviation is very high over this region (Figure 1b) due to
8 pronounced seasonal variations. During NH summer (June/July/August), high CHBr_3 values of
9 around 0.6 ppt are found over a large region stretching from South-East Asia all the way to
10 North-East Africa between 10°N and 25°N . During SH summer (December/January/February),
11 smaller maximum values of around 0.4 ppt CHBr_3 are diagnosed south of India over the Indian
12 Ocean between 5°S - 10°N (Figure 8).

13 In order to evaluate the transport efficiency for oceanic short-lived trace gases in this region,
14 the transit time is calculated from the trajectory analysis for the NH and SH summer seasons.
15 During NH winter, transit times from the surface to the TTL show a very similar pattern as
16 CHBr_3 in the TTL, with shortest transit times of around 45 days over the Indian Ocean
17 coinciding with largest CHBr_3 abundance. During NH summer, on the other hand, the transit
18 times minimize not in the region of maximum CHBr_3 abundance, but instead south of this
19 region where air masses can reach the TTL within 43 days. Between 10°N and 25°N , the
20 transport is still fast and the transit of short lived species from their ocean sources will take
21 around 48 days. Overall the transit time is similar to values found for the West Pacific and
22 cannot solely account for the simulated maximum CHBr_3 values.

23 CHBr_3 contributing to the Indian Ocean TTL maximum mostly stems from the Bay of Bengal,
24 the Arabian Sea, the equatorial region of the Indian Ocean and the coast lines of South-East
25 Asian countries like China. Compared to the oceanic contributions identified for the other two
26 regions, the sources for the Indian Ocean CHBr_3 maxima show a large regional extent including
27 coastal and open ocean emissions from 20°S to 30°N . Given that oceanic emissions from large
28 parts of the Indian Ocean and adjacent coastal areas can be transported into the Asian monsoon
29 region (Fiehn et al., 2017), the CHBr_3 maxima can be explained by the strong oceanic emissions
30 in this region combined with efficient boundary layer –TTL transport.

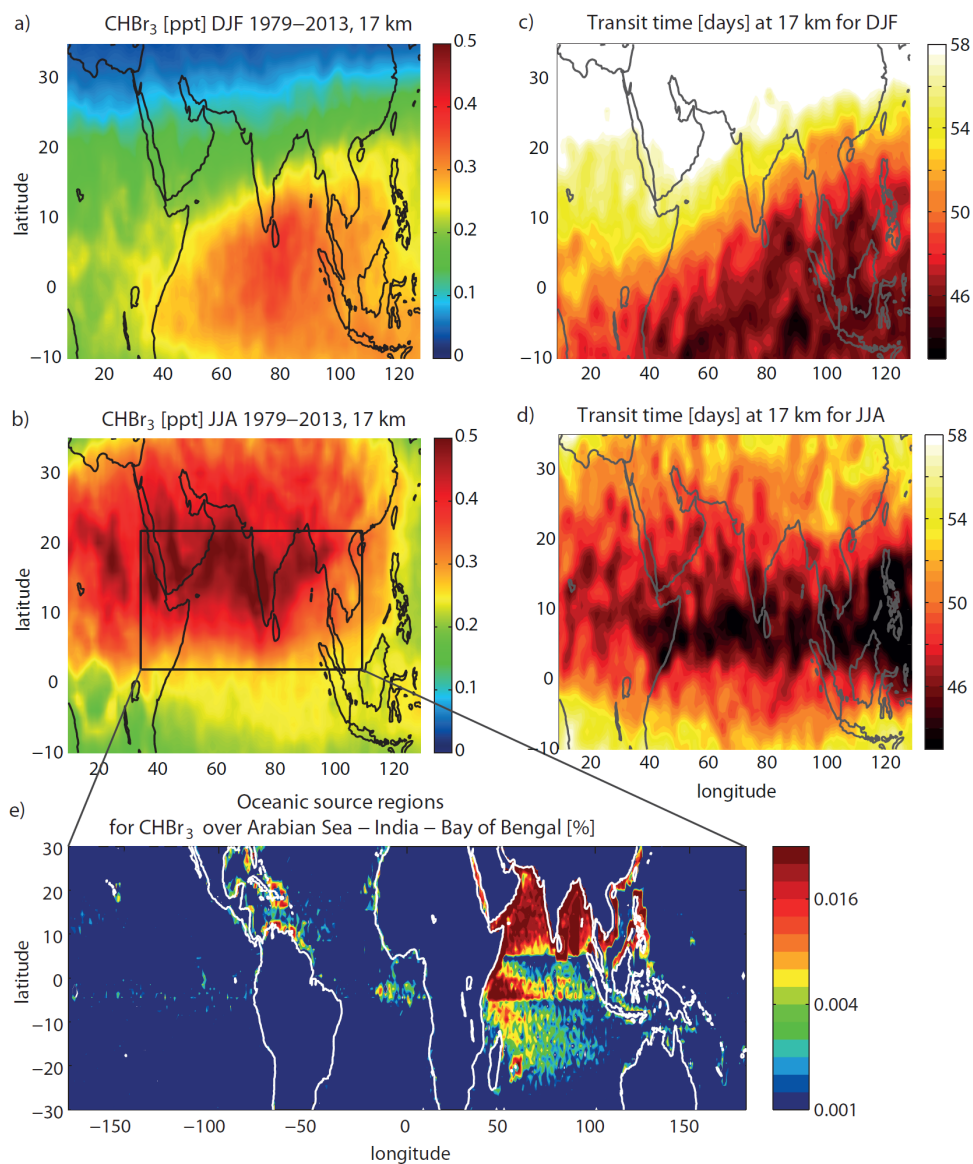


1 The global maxima of CHBr_3 over India, Bay of Bengal and the Arabian Sea is also subject to
2 the largest uncertainties when compared to the other maxima found in our model simulations.
3 For the construction of the emission inventory from Ziska et al. (2013), only one data set was
4 available for the Indian Ocean (Yamamoto et al., 2001). The data set is based on measurements
5 at seven stations in the open ocean waters of the Bay of Bengal and reveals relatively high
6 CHBr_3 values between 8 and 15 ng/L. Given the great distance of the sampling points from the
7 coasts, the authors hypothesized that planktonic production is the most probable source for this
8 high CHBr_3 abundance. Independent measurements from the OASIS campaign in 2014 confirm
9 the subtropical and tropical West Indian Ocean as a strong source for CHBr_3 to the atmosphere,
10 although open ocean surface concentrations were overall lower with maximum values of 8 ng/L
11 (Fiehn et al., 2017). While the high values from Yamamoto et al. (2001) were used locally for
12 the emission climatology, the rest of the tropical Indian Ocean was filled by applying open
13 ocean data from the tropical Atlantic and Pacific. In consequence, the emission scenario for the
14 Indian Ocean has large uncertainties and further VSLS measurements are required to confirm
15 or improve our estimates of the Indian Ocean as the region of strongest CHBr_3 entrainment into
16 the stratosphere.

17

18

19



1

2

3 **Figure 8.** Modeled distribution of CHBr₃ at 17 km for DJF and JJA 1979-2013 (a, b). Transit time of
4 air masses from the ocean surface to the TTL for DJF and JJA (c, d). Oceanic source regions for CHBr₃
5 over Arabian Sea, India and Bay of Bengal (black square in left uppermost panel) at 17 km given in
6 percent per 1°x1° grid box (e).



1 3.5 Interannual and long term changes

2 Long term changes of tropical mean (30°N-30°S) CHBr₃ mixing ratios at 17 km show a weak
3 but significant trend of 0.017 ± 0.012 ppt Br/dec, corresponding to a 10% increase of CHBr₃
4 over the whole time period (1979-2013). Regionally, the long term changes are more
5 pronounced and FLEXPART simulations suggest decreasing or increasing CHBr₃ in the TTL
6 depending on the location (Figure 9). Over South America, Australia and the Central/East
7 Pacific, the trend is not significant given the relatively small trend values compared to the
8 interannual variability found here. For all other regions, CHBr₃ shows a significant, positive
9 trend of 2-10% per decade. CHBr₃ over the Indian Ocean and Maritime continent is highlighted
10 in Figure 9c as the region with the maximum trend (0.04 ppt Br/dec), mostly driven by the
11 ENSO-related steep changes over the time period 2000-2013 (Fiehn et al., 2018). CHBr₃ over
12 the East Pacific is highlighted in Figure 9b as an example of a negative, but not significant trend
13 (-0.017 ppt Br/dec).

14 The projected interannual and long-term changes of CHBr₃ injections are driven by the
15 variability of oceanic emissions (Ziska et al., 2013), convective transport from the surface to
16 the TTL (Aschmann et al., 2011) and transport in the TTL (Krüger et al., 2009). Our model
17 runs are based on CHBr₃ emissions that allow for changes over time due to changing
18 meteorological surface parameters (mostly ERA-Interim), but do not take into account oceanic
19 biogeochemical and related CHBr₃ production changes. Due to increasing sea surface
20 temperature and wind speed, CHBr₃ emissions increase considerably by 7.9% from 1979 to
21 2013 (Ziska et al., 2017). Changes in the modelled atmospheric transport are driven by long-
22 term changes in ERA-Interim parameters such temperature, winds and humidity fields which
23 contribute in addition to the emission to the overall trend of CHBr₃ at 17 km of 10% for 1979-
24 2013.

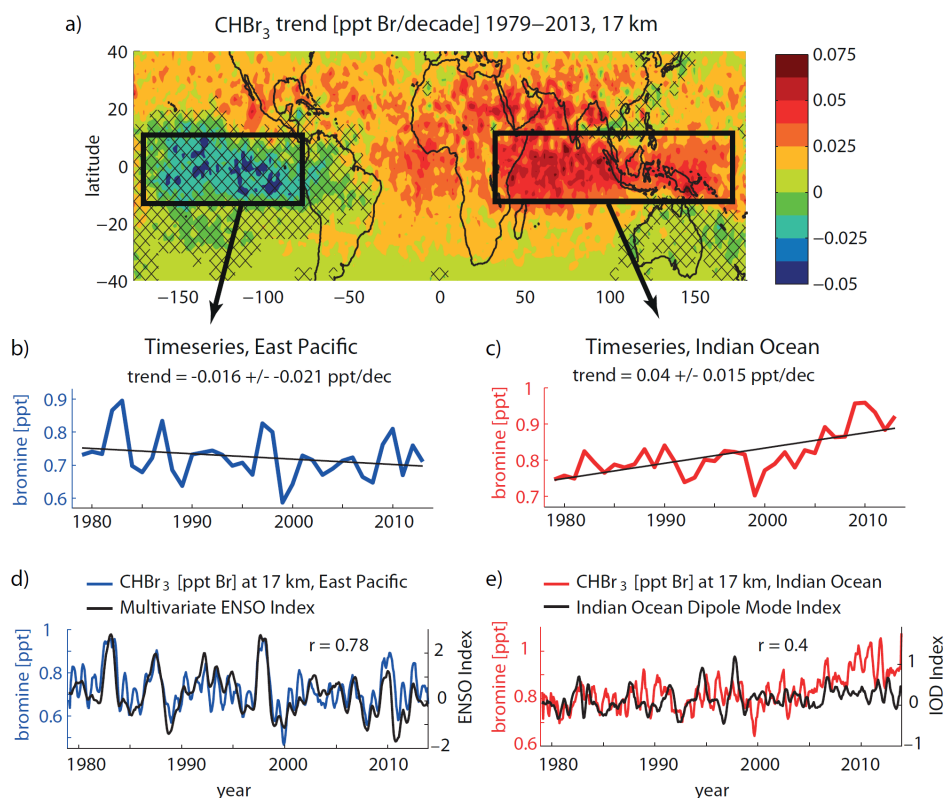
25 The two CHBr₃ time series over the East Pacific and Indian Ocean/Maritime Continent (Figure
26 9b and 9c) show the opposite long-term behaviour, but also share some of the same patterns of
27 interannual variability. In particular, signals like the steep CHBr₃ decrease from 1997/1998 to
28 1999, the increase from 2008 to 2009/2010 and the relatively high values in 1982 are common
29 to both time series. We analyze the common and separate drivers of the variability of the two
30 time series further by comparing them to modes of tropical climate variability.

31 First, we compare the time series of stratospheric bromine in the East Pacific with the
32 Multivariate ENSO Index (MEI; Wolter and Timlin, 2011) in Figure 9d. The irregular ENSO



1 variations in winds and sea surface temperatures over the tropical eastern Pacific Ocean drive
2 changes in CHBr_3 emissions and atmospheric transport leading to a high correlation of the two
3 time series ($r = 0.78$). During El Niño years, water in the Central and Eastern Pacific becomes
4 warmer than usual and the dry and steady easterly winds turn into warm and moist westerlies
5 leading to an increase of the oceanic emissions. This increase is driven by meteorological and
6 oceanic surface variations, but does not allow for possible changes in biogenic CHBr_3
7 production related to changes in the Eastern Pacific upwelling system (Hepach et al., 2016). At
8 the same time the warm East Pacific favors stronger convection intensifying the VLSL transport
9 into the TTL (Aschmann et al., 2011). Overall, El Niño years lead to enhanced CHBr_3 injection
10 over the East Pacific (e.g., 1982, 1986, 1991, and 1997), while La Niña corresponds to weaker
11 CHBr_3 injection (e.g., 1988, and 2010).

12



13

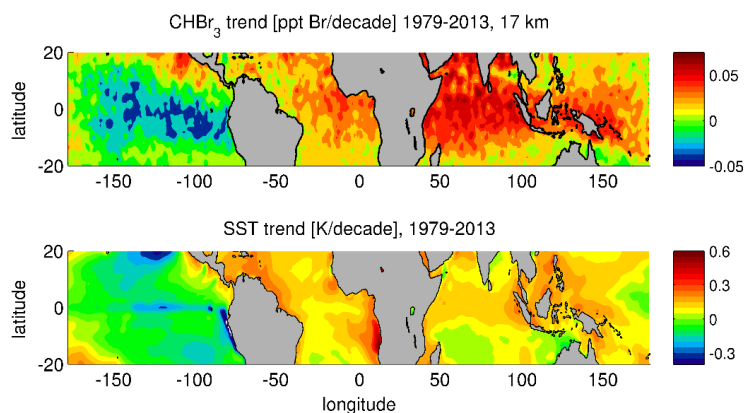
14



1 **Figure 9.** Modeled long-term change of CHBr_3 [Br/decade] at 17 km for the time period 1979-
2 2013 (a). Time series (annual means) averaged over the East Pacific and the Indian
3 Ocean/Maritime continent/West Pacific region are shown together with the trend (b, c). Time
4 series (5 months running mean) are shown together with the ENSO index and Indian Ocean
5 Dipole index, respectively (d, e).

6 Second, variations of CHBr_3 at 17 km over the Indian Ocean and Maritime continent are shown
7 together with the Indian Ocean Dipole (IOD) Mode Index (Figure 9e), an indicator of the east-
8 west temperature gradient across the tropical Indian Ocean (Saji et al., 1999). The two
9 timeseries are weakly correlated ($r=0.4$) sharing some of their variability. The IOD is a coupled
10 ocean-atmosphere phenomenon with anomalous cooling of the south eastern tropical Indian
11 Ocean and anomalous warming of the western tropical Indian Ocean during a positive phase.
12 Associated with these changes the convection normally situated over the eastern Indian Ocean
13 warm pool shifts to the west. For some years, the positive phase results in slightly stronger
14 CHBr_3 emissions and more effective atmospheric transport (e.g., 1982-83, 2006). In other years,
15 strong IOD events will not impact the CHBr_3 abundance over the Indian Ocean/Maritime
16 Continent (e.g., 1997-98). The relatively weak correlation of CHBr_3 injection and IOD results
17 from the influence of the ENSO signal on atmospheric transport in this region. A combination
18 of SST anomalies in the West Indian Ocean and the ENSO signal can have varying impacts on
19 the CHBr_3 injection depending on the time of year (Fiehn et al., 2018). While positive SST
20 anomalies together with El Niño conditions in boreal winter and spring enhance stratospheric
21 VLS injection, La Niña conditions in boreal fall can also cause stronger than normal
22 stratospheric injection. Overall, the inter-annual variability of the CHBr_3 time series is driven
23 by a combination of the ocean-atmosphere modes in the Indian and Pacific Ocean, however,
24 the strong increase during 2009-2013 is not related to either of the two modes.

25



1

2 **Figure 10.** Modeled long-term change of FLEXPART CHBr₃ [ppt Br/decade] at 17 km and
3 ERA-Interim sea surface temperature (SST) [K/decade] for the time period 1979-2013.

4

5 The overall pattern of long-term CHBr₃ changes at 17 km shows a strong similarity to the long-
6 term changes in sea surface temperature derived from ERA-Interim data (Figure 10). While the
7 global mean surface temperature has increased due to anthropogenic greenhouse gas emissions
8 (Hegerl et al., 2007), the spatial pattern of global warming is more complex. Most regions
9 exhibit a warming trend over the 35 year period, however, much of the eastern Pacific cooled.
10 This cooling may either be related to an unusual strong manifestation of internal variability in
11 the observations or may be caused by external, regional forcings (e.g., Wang et al., 2012; Luo
12 et al., 2012). ERA-Interim long-term temperature changes over the tropical oceans show good
13 agreement with HadCRUT, a combined dataset of instrumental temperature records, with only
14 small differences (Simmons et al., 2014). Most interesting for our analysis is the correlation
15 between the SST trends and the long-term changes of stratospheric CHBr₃ entrainment. Regions
16 with large positive SST trends such as the Indian Ocean, East Atlantic and Maritime Continent
17 coincide with regions where the CHBr₃ entrainment trend is strongest. The east Pacific, on the
18 other hand, stands out as the region where the SST cooling trend coincides with decreasing
19 CHBr₃ entrainment. While this relation holds for many oceanic regions, we also find outliers
20 such as the southern Indian Ocean, where SST trends are around zero but CHBr₃ entrainment
21 shows a strong positive trend. Based on our modelling approach, the interaction of two
22 mechanisms causes the strong correlation between the SST and CHBr₃ trends. Higher sea
23 surface temperatures and stronger surface winds force a larger flux of CHBr₃ out of the ocean



1 into the atmosphere (Ziska et al., 2013) and at the same time cause enhanced convection,
2 transporting surface air masses into the TTL (Tegtmeier et al., 2015). As the cold point
3 tropopause altitude shows no significant trend in radiosondes or ERA-Interim data over the
4 1980-2013 time period (Tegtmeier et al., 2019), CHBr_3 changes at 17 km correspond directly to
5 changes of stratospheric CHBr_3 entrainment. Future SST changes can be expected to drive a
6 continued positive trend of stratospheric CHBr_3 entrainment (Hossaini et al., 2012a).

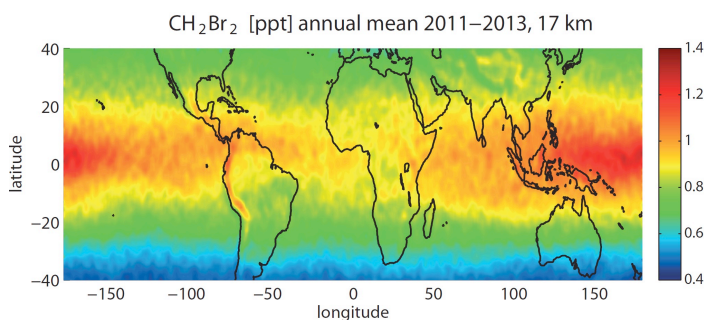


1 3.6 Overall CH₂Br₂ and CHBr₃ contribution to stratospheric bromine

2

3 CHBr₃ together with CH₂Br₂ provides the main contribution of oceanic bromine to the
4 stratosphere. CH₂Br₂ mixing ratios in the inner tropical belt (10°S-10°N) show less variability
5 than CHBr₃, consistent with the longer lifetime, and range between 0.9 and 1.4 ppt. Largest
6 values can be detected over the West and Central Pacific and are distributed evenly over both
7 hemispheres (Figure 11). There is no local CH₂Br₂ maxima over the Indian Ocean, as observed
8 for CHBr₃, since no strong localized sources in the region exist according to the Ziska et al.,
9 (2013) climatology. However, new ship measurements in the western Indian Ocean revealed
10 high CH₂Br₂ surface water concentrations, i.e., south of Madagascar in July 2011 (Fiehn et al.,
11 2017). Seasonal and interannual variations of CH₂Br₂ are much weaker than for CHBr₃ resulting
12 in a continuous bromine entrainment into the stratosphere.

13



14

15

16 **Figure 11.** Modeled tropical annual mean distribution of CH₂Br₂ [ppt] at 17 km for 2011-2013.

17

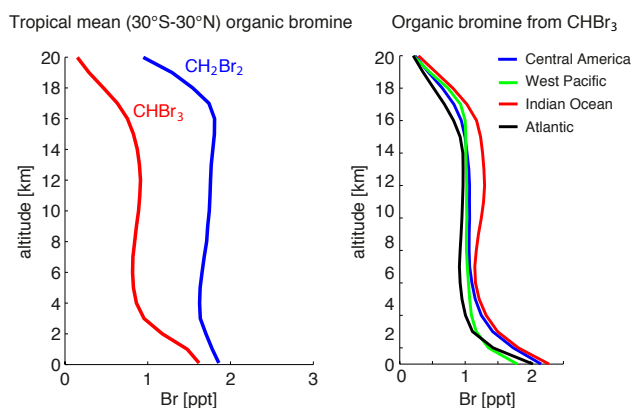
18 Figure 12 shows the annual tropical mean CHBr₃ and CH₂Br₂ averaged over 1979-2013. At the
19 surface, tropical mean values of 1 ppt CH₂Br₂ and 0.6 ppt CHBr₃ are simulated which are
20 slightly smaller than reported observations (Ziska et al., 2013 and references therein). Mixing
21 ratios in the free troposphere decrease by nearly 50% (10%) for CHBr₃ (CH₂Br₂) when
22 compared to the marine boundary layer. Both gases are well mixed in the free troposphere with
23 nearly constant mixing ratios of 0.3 and 0.9 ppt for CHBr₃ and CH₂Br₂, respectively,
24 corresponding to 0.9 ppt and 1.8 ppt bromine (Figure 12). CHBr₃ shows a slight S-shape with



1 elevated abundances around 12-14 km related to strong convective outflow at this level bringing
2 marine boundary layer air directly into the lower TTL. Above 14 km, CHBr_3 mixing ratios start
3 to decrease reaching values of 0.22 ppt at 17 km close to the cold point, corresponding to 0.66
4 ppt bromine. CH_2Br_2 mixing ratios, on the other hand, stay nearly constant up to 18 km, as
5 expected based on its quite long lifetime of 400 to 500 days in the TTL, reaching values of 0.9
6 ppt (1.8 ppt bromine).

7 CHBr_3 profiles for four different regions show that surface atmospheric mixing ratios are
8 strongest in the Indian Ocean and Central America. Overall maximum mixing ratios over the
9 Indian Ocean result from such strong surface emissions combined with a relatively strong
10 transport and main convective outflow between 11 and 14 km giving an S-shape CHBr_3 profile.
11 Only for the West Pacific, transport into the stratosphere is more efficient, however, smaller
12 emissions result in only second largest entrainment over this region.

13



14

15 **Figure 12.** Modeled vertical profiles of CHBr_3 and CH_2Br_2 [ppt Br] in the tropics (30°S-30°N)
16 (right panel) and of CHBr_3 for Central America (0°-20°N, 70°W-110°W), West Pacific (15°S-
17 5°N, 140°E-150°W), Indian Ocean (0°-20°N, 40°E-110°E), and Atlantic (0°-20°N, 20°W-
18 50°W) (right panel) for 1979-2013.

19

20 Table 2 gives the contribution of CHBr_3 and CH_2Br_2 to the stratospheric bromine loading based
21 on source gas (SG) injection alone, and based on the sum of source and product gas (PG)
22 injection. CHBr_3 and CH_2Br_2 have been evaluated directly at the cold point (as given by ERA-



1 Interim) and contribute 2.4 ppt Br to stratospheric bromine loading directly in form of SG
2 entrainment with 75% (25%) resulting from CH₂Br₂ (CHBr₃). The CHBr₃ estimates of 0.2 ppt
3 (corresponding to 0.6 ppt Br) are in agreement with other studies which range from 0.1 ppt
4 (Warwick et al., 2006; Aschmann et al., 2009) to 0.35 ppt (Hossaini et al., 2012b). For CH₂Br₂,
5 our results of 0.9 ppt (corresponding to 1.8 ppt Br) agree very well with CTM modeling studies
6 (Hossaini et al., 2012b) which give estimates of 0.75 – 0.9 ppt. The overall contribution of the
7 two gases in form of SG and PG entrainment of 4.7 ppt is also in good agreement with earlier
8 studies giving estimates ranging from 4-5 ppt (Hossaini et al., 2013) to 7.7 ppt (Liang et al.,
9 2014). Considering that CH₂Br₂ and CHBr₃ contribute >80% of the total SG Br in the TTL, our
10 estimates also agree well with measurements and model calculations reported in Navarro et al.
11 (2015) and Wales et al. (2018). Navarro et al. (2015) reported measurements at the tropopause
12 (17 km) of total VSL-Br of 5.24 ± 0.51 ppt in the Western tropical Pacific and 5.98 ± 1.95 ppt
13 in the Eastern tropical Pacific. Modeled PG for these conditions varied between 38 and 50%
14 of the total VSL-Br. Also, Wales et al. (2018) estimated at total of 5.0 ± 2.1 ppt of total VSL-
15 Br at the tropical Western Pacific Tropopause, which included 2.9 ± 0.6 ppt of SG Br and 2.1
16 ± 2.1 ppt of PG Br.

17

18 **Table 2.** Modeled contribution of CHBr₃ and CH₂Br₂ to the stratospheric halogen loading in
19 form of source gas (SG) and total (SG+PG) contribution for 2011-2013.

Br [ppt]	Inner tropics (10°S-10°N)		Tropics (30°S-30°N)	
	SG	SG+PG	SG	SG+PG
CHBr ₃	0.9	1.1	0.6	0.9
CH ₂ Br ₂	2.1	4.4	1.8	3.8
CHBr₃ + CH₂Br₂	3.0	5.5	2.4	4.7

20

21



1 **4 Discussion and summary**

2

3 We combine observational data sets, including surface and upper air measurements, with high
4 resolution atmospheric modelling in order to analyze the spatial and temporal variability of
5 VLSL entrainment into the stratosphere. Oceanic CHBr₃ in the TTL, on its way from the marine
6 boundary layer into the stratosphere, shows a very high spatial and temporal variability.
7 Regional maxima with mixing ratios of up to 0.4 to 0.5 ppt are simulated to be over Central
8 America (1) and the Maritime continent and tropical West Pacific (2), both of which are
9 confirmed by high-altitude aircraft campaigns. The strongest stratospheric CHBr₃ entrainment
10 is projected to occur over the region of India, Bay of Bengal and Arabian Sea (3), however, no
11 data from aircraft campaigns are available to confirm this finding. Other tropical regions with
12 only little convective uplift show smaller mixing ratios, mostly between 0.1 and 0.2 ppt. CHBr₃
13 fields on daily mean or shorter time scales is characterized by pronounced spatial variations
14 with highly localized injections.

15 The modelled CHBr₃ maximum over Central America is caused by the co-occurrence of
16 convectively-driven short transport time scales and strong regional sources, with the latter being
17 confirmed by data from various ship campaigns. Moreover, the combined seasonality of
18 transport efficiency and emission strength causes the strong seasonality of CHBr₃ at 17km over
19 Central America. The model simulations also show a high spatial variability of CHBr₃ with
20 strong latitudinal gradients, which is confirmed by available aircraft campaigns. The
21 comparisons reveal that our model results are similar to the measurements for NH winter, but
22 over- and underestimate (depending on the campaign) observations during NH summer, when
23 the variability is largest. Exceptionally high CHBr₃ observed during the ACCENT campaign
24 is also evident in the model results, but only in the daily and not in the monthly mean values.
25 Given that individual campaigns may not be representative of mean values, but may rather
26 describe one side of the large spectrum, differences between model simulations and
27 measurements, such as the ones discussed above, have to be interpreted with caution.

28 The modelled CHBr₃ maximum in the TTL over the West Pacific is centered south of the
29 equator. This distribution cannot be explained by transport times scales, which are similar north
30 and south of the equator and do not reveal strong hemispheric differences. Instead, strong
31 oceanic sources south of equator, prescribed based on limited available measurements, are
32 responsible for the high CHBr₃ mixing ratios in the SH. Measurements in the upper TTL from



1 the ATTREX aircraft campaign show an overall good agreement with model results, but also
2 indicate that the model underestimates CHBr_3 in the NH tropics. Furthermore, ATTREX
3 measurements did not show any significant gradient between the NH and SH tropics near the
4 tropopause. Given the scarcity of in-situ measurements in the open ocean water of the West
5 Pacific, it may be possible that oceanic emissions estimates used here are too low north of the
6 equator. Future ship campaigns are needed to confirm spatial and temporal differences and to
7 improve existing bottom-up emission climatologies.

8 The overall strongest maximum over India, Bay of Bengal and Arabian Sea is caused by very
9 large local sources. Transport from the ocean surface to 17 km is also efficient, but not strong
10 enough to solely explain the pronounced maxima. No upper air measurements are available to
11 back this upper TTL maximum and oceanic measurements used for the emission scenarios are
12 also scarce. For the global tropical/extratropical distribution of CHBr_3 entrainment, largest
13 uncertainties exist for estimated maxima in the region over India, Bay of Bengal and Arabian
14 Sea. In situ measurements of the oceanic sources and the atmospheric distribution are needed
15 to reduce local uncertainties and confirm global mean values.

16 Interannual variability of stratospheric CHBr_3 entrainment is to a large part driven by the
17 variability of the coupled ocean-atmosphere circulation systems such as ENSO in the Pacific
18 and IOD in the Indian Ocean. Long-term trends of the CHBr_3 entrainment, on the other hand,
19 show a pronounced correlation with the SST trends. Both relations are based on the fact the
20 stratospheric CHBr_3 entrainment is driven by strong sources and convective entrainment, which
21 maximize for high surface temperatures and strong wind speeds. Following the SST trends,
22 long term changes of CHBr_3 entrainment are positive in the West Pacific and Asian monsoon
23 region but negative in the East Pacific. The tropical mean trend accounts for an increase of
24 0.017 ± 0.012 ppt Br/dec resulting in a 10% increase over the 1979-2013 time period. The overall
25 contribution of CHBr_3 and CH_2Br_2 to the stratospheric halogen loading is 4.7 ppt Br with 50%
26 being entrained in form of source gases, and the other 50% being entrained in form of product
27 gases.

28

29



1 **Data availability.** The bromoform emission inventory data (Ziska et al., 2013) are available at
2 ACP/Pangaea and the FLEXPART model output can be inquired about by contacting the
3 authors.

4 **Author contributions.** ST, KK, and BQ developed the idea for this paper and the model
5 experiments. ST carried out the FLEXPART model calculations and the comparison to the
6 aircraft observations. EA provided aircraft data. FZ compiled the Ziska et al. (2013) climatology
7 for this study. ST wrote the manuscript with contributions from all co-authors.

8 **Competing interests.** The authors declare that they have no conflict of interest.

9 **Acknowledgements** This study was carried out within the BMBF project ROMIC THREAT
10 (01LG1217A). ST was funded by ROMIC THREAT (01LG1217A) when compiling the study
11 and is currently supported by the Deutsche Forschungsgemeinschaft (DFG, German Research
12 Foundation) – TE 1134/1. EA was supported by grants from the NASA Upper Atmosphere.
13 The authors are grateful to the ECMWF for making the reanalysis product ERA-Interim
14 available.



1 **References**

- 2 Aschmann, J., Sinnhuber, B.-M., Atlas, E. L. and Schauffler, S. M.: Modeling the transport of
3 very short-lived substances into the tropical upper troposphere and lower stratosphere,
4 *Atmospheric Chemistry and Physics*, 9(23), 2009.
- 5 Aschmann, J., Sinnhuber, B.-M., Chipperfield, M. P., and Hossaini, R.: Impact of deep
6 convection and dehydration on bromine loading in the upper troposphere and lower
7 stratosphere, *Atmos. Chem. Phys.*, 11, 2671-2687, <https://doi.org/10.5194/acp-11-2671-2011>,
8 2011.
- 9 Austin, J., N., and Butchart, N.: Coupled chemistry-climate model simulations for the period
10 1980 to 2020: ozone depletion and the start of ozone recovery, *Quarterly Journal of the Royal*
11 *Meteorological Society*, 129: 3225–3249, 2006.
- 12 Braesicke, P., Keeble, J., Yang, X., Stiller, G., Kellmann, S., Abraham, N. L., Archibald, A.,
13 Telford, P., and Pyle, J. A.: Circulation anomalies in the Southern Hemisphere and ozone
14 changes, *Atmos. Chem. Phys.*, 13, 10677–10688, [doi:10.5194/acp-13-10677-2013](https://doi.org/10.5194/acp-13-10677-2013), 2013.
- 15 Brinckmann, S., Engel, A., Bönisch, H., Quack, B., and Atlas, E.: Short-lived brominated
16 hydrocarbons – observations in the source regions and the tropical tropopause layer, *Atmos.*
17 *Chem. Phys.*, 12, 1213-1228, [doi:10.5194/acp-12-1213-2012](https://doi.org/10.5194/acp-12-1213-2012), 2012.
- 18 Butler, J. H., King, D. B., Lobert, J. M., Montzka, S. A., Yvon-Lewis, S. A., Hall, B. D.,
19 Warwick, N. J., Mondeel, D. J., Aydin, M. and Elkins, J. W.: Oceanic distributions and
20 emissions of short-lived halocarbons, *Global Biogeochemical Cycles*, 21(1),
21 [doi:10.1029/2006GB002732](https://doi.org/10.1029/2006GB002732), 2007.
- 22 Carpenter, L.J. and Reimann, S. (Lead Authors), J.B. Burkholder, C. Clerbaux, B.D. Hall, R.
23 Hossaini, J.C. Laube, and S.A. Yvon-Lewis, Ozone-Depleting Substances (ODSs) and Other
24 Gases of Interest to the Montreal Protocol, Chapter 1 in *Scientific Assessment of Ozone*
25 *Depletion: 2014*, Global Ozone Research and Monitoring Project–Report No. 55, World
26 Meteorological Organization, Geneva, Switzerland, 2014.
- 27 Chipperfield, M. P.: New version of the TOMCAT/SLIMCAT off-line chemical transport
28 model: Intercomparison of stratospheric tracer experiments, *Quarterly Journal of the Royal*
29 *Meteorological Society*, 132(617), 1179–1203, [doi:10.1256/qj.05.51](https://doi.org/10.1256/qj.05.51), 2006.
- 30 Dee, D. P., Uppala, S. M., Simmons, A. J., Berrisford, P., Poli, P., Kobayashi, S., Andrae, U.,
31 Balmaseda, M. A., Balsamo, G., Bauer, P., Bechtold, P., et al.: The ERA-Interim reanalysis:
32 configuration and performance of the data assimilation system, *Quarterly Journal of the Royal*
33 *Meteorological Society*, 137(656), 553–597, [doi:10.1002/qj.828](https://doi.org/10.1002/qj.828), 2011.
- 34 Dorf, M., Butz, A., Camy-Peyret, C., Chipperfield, M. P., Kritten, L., and Pfeilsticker, K.:
35 Bromine in the tropical troposphere and stratosphere as derived from balloon-borne BrO
36 observations, *Atmos. Chem. Phys.*, 8, 7265-7271, [doi:10.5194/acp-8-7265-2008](https://doi.org/10.5194/acp-8-7265-2008), 2008.



- 1 Fiehn, A., Quack, B., Hepach, H., Fuhlbrügge, S., Tegtmeier, S., Toohey, M., Atlas, E., and
2 Krüger, K.: Delivery of halogenated very short-lived substances from the west Indian Ocean to
3 the stratosphere during the Asian summer monsoon, *Atmos. Chem. Phys.*, 17, 6723-6741,
4 <https://doi.org/10.5194/acp-17-6723-2017>, 2017.
- 5 Fiehn, A., Quack, B., Marandino, C. A., and Krüger, K., Transport variability of very short
6 lived substances from the West Indian Ocean to the stratosphere. *Journal of Geophysical*
7 *Research: Atmospheres*, 123, 5720– 5738. <https://doi.org/10.1029/2017JD027563>, 2018.
- 8 Forster, C., Stohl, A. and Seibert, P.: Parameterization of Convective Transport in a Lagrangian
9 Particle Dispersion Model and Its Evaluation, *Journal of Applied Meteorology and*
10 *Climatology*, 46(4), 403–422, doi:10.1175/JAM2470.1, 2007.
- 11 Forster, C., Wandinger, U., Wotawa, G., James, P., Mattis, I., Althausen, D., Simmonds, P.,
12 O’Doherty, S., Jennings, S. G., Kleefeld, C., Schneider, J., et al.: Transport of boreal forest fire
13 emissions from Canada to Europe, *Journal of Geophysical Research*, 106(D19), 22887,
14 doi:10.1029/2001JD900115, 2001.
- 15 Fuhlbrügge, S., Quack, B., Tegtmeier, S., Atlas, E., Hepach, H., Shi, Q., Raimund, S., and
16 Krüger, K.: The contribution of oceanic halocarbons to marine and free tropospheric air over
17 the tropical West Pacific, *Atmos. Chem. Phys.*, 16, 7569-7585, [https://doi.org/10.5194/acp-16-](https://doi.org/10.5194/acp-16-7569-2016)
18 [7569-2016](https://doi.org/10.5194/acp-16-7569-2016), 2016.
- 19 Hegerl, G.C., F. W. Zwiers, P. Braconnot, N.P. Gillett, Y. Luo, J.A. Marengo Orsini, N.
20 Nicholls, J.E. Penner and P.A. Stott: Understanding and Attributing Climate Change. In:
21 *Climate Change 2007: The Physical Science Basis. Contribution of Working Group I to the*
22 *Fourth Assessment Report of the Intergovernmental Panel on Climate Change [Solomon, S., D.*
23 *Qin, M. Manning, Z. Chen, M. Marquis, K.B. Averyt, M. Tignor and H.L. Miller (eds.)].*
24 Cambridge University Press, Cambridge, United Kingdom and New York, NY, USA, 2007
- 25 Hepach, H., Quack, B., Tegtmeier, S., Engel, A., Bracher, A., Fuhlbrügge, S., Galgani, L.,
26 Atlas, E. L., Lampel, J., Frieß, U., and Krüger, K.: Biogenic halocarbons from the Peruvian
27 upwelling region as tropospheric halogen source, *Atmos. Chem. Phys.*, 16, 12219-12237,
28 <https://doi.org/10.5194/acp-16-12219-2016>, 2016.
- 29 Hossaini, R., Chipperfield, M. P., Dhomse, S., Ordóñez, C., Saiz-Lopez, A., Abraham, N. L.,
30 Archibald, A. T., Braesicke, P., Telford, P., and Warwick, N.: Modelling future changes to the
31 stratospheric source gas injection of biogenic bromocarbons, *Geophys. Res. Lett.*, 39, L20813,
32 doi: 10.1029/2012GL053401, 2012a.
- 33 Hossaini, R., Chipperfield, M. P., Feng, W., Breider, T. J., Atlas, E., Montzka, S. A., Miller, B.
34 R., Moore, F. and Elkins, J.: The contribution of natural and anthropogenic very short-lived
35 species to stratospheric bromine, *Atmospheric Chemistry and Physics*, 12(1), 371–380,
36 doi:10.5194/acp-12-371-2012, 2012b.



- 1 Hossaini, R., Mantle, H., Chipperfield, M. P., Montzka, S. A., Hamer, P., Ziska, F., Quack, B.,
2 Krüger, K., Tegtmeier, S., Atlas, E., Sala, S., Engel, A., Bönisch, H., Keber, T., Oram, D., Mills,
3 G., Ordóñez, C., Saiz-Lopez, A., Warwick, N., Liang, Q., Feng, W., Moore, F., Miller, B. R.,
4 Marécal, V., Richards, N. A. D., Dorf, M., and Pfeilsticker, K.: Evaluating global emission
5 inventories of biogenic bromocarbons, *Atmos. Chem. Phys.*, 13, 11819-11838,
6 doi:10.5194/acp-13-11819-2013, 2013.
- 7 Hossaini, R., Chipperfield, M. P., Montzka, S. A., Rap, A., Dhomse, S., and Feng, W.:
8 Efficiency of short-lived halogens at influencing climate through depletion of stratospheric
9 ozone, *Nat. Geosci.*, 8, 186–190, doi:10.1038/ngeo2363, 2015.
- 10 Hossaini, R., Patra, P. K., Leeson, A. A., Kryzstofiak, G., Abraham, N. L., Andrews, S. J.,
11 Archibald, A. T., Aschmann, J., Atlas, E. L., Belikov, D. A., Bönisch, H., Carpenter, L. J.,
12 Dhomse, S., Dorf, M., Engel, A., Feng, W., Fuhlbrügge, S., Griffiths, P. T., Harris, N. R. P.,
13 Hommel, R., Keber, T., Krüger, K., Lennartz, S. T., Maksyutov, S., Mantle, H., Mills, G. P.,
14 Miller, B., Montzka, S. A., Moore, F., Navarro, M. A., Oram, D. E., Pfeilsticker, K., Pyle, J.
15 A., Quack, B., Robinson, A. D., Saikawa, E., Saiz-Lopez, A., Sala, S., Sinnhuber, B.-M.,
16 Taguchi, S., Tegtmeier, S., Lidster, R. T., Wilson, C., and Ziska, F.: A multi-model
17 intercomparison of halogenated very short-lived substances (TransCom-VSLS): linking
18 oceanic emissions and tropospheric transport for a reconciled estimate of the stratospheric
19 source gas injection of bromine, *Atmos. Chem. Phys.*, 16, 9163-9187, doi:10.5194/acp-16-
20 9163-2016, 2016.
- 21 Ko, M.K.W. and Poulet, G. (Lead Authors) Blake, D.R., Boucher, O., Burkholder, J.H., Chin,
22 M., Cox, R.A., George, C., Graf, H.-F., Holton, J.R., Jacob, D.J., Law, K.S., Lawrence, M.G.,
23 Midgley, P.M., Seakins, P.W., Shallcross, D.E., Strahan, S.E., Wuebbles, D.J., and Yokouchi,
24 Y. (2002) Very short-lived halogen and sulfur substances. Chapter 2 in Scientific Assessment
25 of Ozone Depletion: 2002 Global Ozone Research and Monitoring Project–Report No. 47,
26 World Meteorological Organization, Geneva, Switzerland, 2003.
- 27 Krüger, K., Tegtmeier, S. and Rex, M.: Variability of residence time in the Tropical Tropopause
28 Layer during Northern Hemisphere winter, *Atmos. Chem. Phys.*, 9(18), 6717–6725, 2009.
- 29 Liang, Q., Stolarski, R. S., Kawa, S. R., Nielsen, J. E., Douglass, A. R., Rodriguez, J. M., Blake,
30 D. R., Atlas, E. L., and Ott, L. E.: Finding the missing stratospheric Br_y: a global modeling
31 study of CHBr₃ and CH₂Br₂, *Atmos. Chem. Phys.*, 10, 2269-2286, doi:10.5194/acp-10-2269-
32 2010, 2010.
- 33 Liang, Q., Atlas, E., Blake, D., Dorf, M., Pfeilsticker, K., and Schauffler, S.: Convective
34 transport of very short lived bromocarbons to the stratosphere, *Atmos. Chem. Phys.*, 14, 5781-
35 5792, https://doi.org/10.5194/acp-14-5781-2014, 2014.
- 36 Luo, J. J., W. Sasak ia, and Y. Masumoto: Indian Ocean warming modulates Pacific climate
37 change, *Proc. Natl. Acad. Sci. U.S.A.*, 109, 18,701–18,706, doi:10.1073/pnas.1210239109,
38 2012.



- 1 Marandino, C. A., Tegtmeier, S., Krüger, K., Zindler, C., Atlas, E. L., Moore, F., and Bange,
2 H. W.: Dimethylsulphide (DMS) emissions from the western Pacific Ocean: a potential marine
3 source for stratospheric sulphur?, *Atmos. Chem. Phys.*, 13, 8427–8437,
4 <https://doi.org/10.5194/acp-13-8427-2013>, 2013.
- 5 McLinden, C. A., Haley, C. S., Lloyd, N. D., Hendrick, F., Rozanov, A., Sinnhuber, B.-M.,
6 Goutail, F., Degenstein, D. A., Llewellyn, E. J., Sioris, C. E., Van Rozendaal, M., Pommereau,
7 J. P., Lotz, W., and Burrows, J. P.: Odin/OSIRIS observations of stratospheric BrO: Retrieval
8 methodology, climatology, and inferred Bry, *J. Geophys. Res.-Atmos.*, 115, D15308,
9 [doi:10.1029/2009JD012488](https://doi.org/10.1029/2009JD012488), 2010.
- 10 Navarro, M. A., Atlas, E. L., Saiz-Lopez, A., Rodriguez-Lloveras, X., Kinnison, D. E.,
11 Lamarque, J.-F., Tilmes, S., Filus, M., Harris, N. R., and Meneguz, E.: Airborne measurements
12 of organic bromine compounds in the Pacific tropical tropopause layer, *P. Natl. Acad. Sci. USA*,
13 112, 13789–13793, 2015.
- 14 Nightingale, P. D., Malin, G., Law, C. S., Watson, A. J., Liss, P. S., Liddicoat, M. I., Boutin, J.
15 and Upstill-Goddard, R. C.: In situ evaluation of air-sea gas exchange parameterizations using
16 novel conservative and volatile tracers, *Global Biogeochemical Cycles*, 14(1), 373–387,
17 [doi:10.1029/1999GB900091](https://doi.org/10.1029/1999GB900091), 2000.
- 18 Ordóñez, C., Lamarque, J.-F., Tilmes, S., Kinnison, D. E., Atlas, E. L., Blake, D. R., Sousa
19 Santos, G., Brasseur, G. and Saiz-Lopez, A.: Bromine and iodine chemistry in a global
20 chemistry-climate model: description and evaluation of very short-lived oceanic sources,
21 *Atmospheric Chemistry and Physics*, 12(3), 1423–1447, [doi:10.5194/acp-12-1423-2012](https://doi.org/10.5194/acp-12-1423-2012), 2012.
- 22 Pisso, I., Haynes, P. H., and Law, K. S.: Emission location dependent ozone depletion potentials
23 for very short-lived halogenated species, *Atmos. Chem. Phys.*, 10, 12025–12036,
24 [doi:10.5194/acp-10-12025-2010](https://doi.org/10.5194/acp-10-12025-2010), 2010.
- 25 Pyle, J. A., N. Warwick, X. Yang, P. J. Young, and G. Zeng: Climate/chemistry feedbacks and
26 biogenic emissions, *Philos. Trans. R. Soc. A*, 365(1856), 1727–1740,
27 [doi:10.1098/rsta.2007.2041](https://doi.org/10.1098/rsta.2007.2041), 2007.
- 28 Quack, B., Wallace, D.W.R.: Air-sea flux of bromoform: Controls, rates, and implications.
29 *Global Biogeochemical Cycles*, 17 (1), art. no.-GB1023, 2003.
- 30 Quack, B., E. Atlas, G. Petrick, and D. W. R. Wallace: Bromoform and dibromomethane above
31 the Mauritanian upwelling: Atmospheric distributions and oceanic emissions, *J. Geophys. Res.*,
32 112(D9), D09312, [doi:10.1029/2006JD007614](https://doi.org/10.1029/2006JD007614), 2007.
- 33 Randel, W. J., Park, M., Emmons, L., Kinnison, D., Bernath, P., Walker, K. A., Boone, C., and
34 Pumphrey, H.: Asian Monsoon Transport of Pollution to the Stratosphere, *Science*, 328, 611–
35 613, [doi:10.1126/science.1182274](https://doi.org/10.1126/science.1182274), 2010.



- 1 Saji, N. H., Goswami, B. N., Vinayachandran, P. N., and Yamagata, T.: A dipole made in the
2 Tropical Indian Ocean. *Nature*. 401. 360-3. 10.1038/43854, 1999.
- 3 Salawitch, R. J.: Atmospheric chemistry: biogenic bromine, *Nature*, 439, 275–277, 2006.
- 4 Simmons, A. J., Poli, P., Dee, D. P., Berrisford, P., Hersbach, H., Kobayashi, S. and Peubey,
5 C.: Estimating low-frequency variability and trends in atmospheric temperature using ERA-
6 Interim. *Q.J.R. Meteorol. Soc.*, 140: 329-353. doi:10.1002/qj.2317, 2014.
- 7 Sinnhuber, B., and S. Meul: Simulating the impact of emissions of brominated very short lived
8 substances on past stratospheric ozone trends. *Geophys. Res. Lett.*, 42, 2449–2456. doi:
9 10.1002/2014GL062975, 2015.
- 10 Sioris, C. E., et al.: Latitudinal and vertical distribution of bromine monoxide in the lower
11 stratosphere from Scanning Imaging Absorption Spectrometer for Atmospheric Chartography
12 limb scattering measurements, *J. Geophys. Res.*, 111, D14301, doi: 10.1029/2005JD006479,
13 2006.
- 14 Stemmler, I., Hense, I., and Quack, B.: Marine sources of bromoform in the global open ocean
15 – global patterns and emissions, *Biogeosciences*, 12, 1967-1981, [https://doi.org/10.5194/bg-12-](https://doi.org/10.5194/bg-12-1967-2015)
16 [1967-2015](https://doi.org/10.5194/bg-12-1967-2015), 2015.
- 17 Stohl, A., Forster, C., Frank, A., Seibert, P. and Wotawa, G.: Technical note: The Lagrangian
18 particle dispersion model FLEXPART version 6.2, *Atmospheric Chemistry and Physics*, 5(9),
19 2005.
- 20 Stohl, A., Hittenberger, M., and Wotawa, G.: Validation of the Lagrangian particle dispersion
21 model FLEXPART against large-scale tracer experiment data, *Atmos. Environ.*, 32, 4245–
22 4264, 1998.
- 23 Stohl, A. and Thomson, D. J.: A density correction for Lagrangian particle dispersion models,
24 *BOUNDARY-LAYER METEOROLOGY*, 90(1), 155–167, doi:10.1023/A:1001741110696,
25 1999.
- 26 Stohl, A. and Trickl, T.: A textbook example of long-range transport: Simultaneous observation
27 of ozone maxima of stratospheric and North American origin in the free troposphere over
28 Europe, *Journal of Geophysical Research*, 104(D23), 30445, doi:10.1029/1999JD900803,
29 1999.
- 30 Tegtmeier, S., Krüger, K., Quack, B., Atlas, E. L., Pissò, I., Stohl, A. and Yang, X.: Emission
31 and transport of bromocarbons: from the West Pacific ocean into the stratosphere, *Atmospheric*
32 *Chemistry and Physics*, 12(22), 10633–10648, doi:10.5194/acp-12-10633-2012, 2012.
- 33 Tegtmeier, S., Krüger, K., Quack, B., Atlas, E., Blake, D. R., Boenisch, H., Engel, A., Hepach,
34 H., Hossaini, R., Navarro, M. A., Raimund, S., Sala, S., Shi, Q., and Ziska, F.: The contribution
35 of oceanic methyl iodide to stratospheric iodine, *Atmos. Chem. Phys.*, 13, 11869-11886,
36 <https://doi.org/10.5194/acp-13-11869-2013>, 2013.



- 1 Tegtmeier, S., Ziska, F., Pisso, I., Quack, B., Velders, G. J. M., Yang, X., and Krüger, K.:
2 Oceanic bromoform emissions weighted by their ozone depletion potential, *Atmos. Chem.*
3 *Phys.*, 15, 13647-13663, doi:10.5194/acp-15-13647-2015, 2015.
- 4 Tegtmeier, S., Davis, S., Dragani, R., Harada, Y., Ivanciu, I., Pilch Kedzierski, R., Krüger, K.,
5 Legras, B., Long, C., Wang, J. S., Wargan, K., and Wright, J. S., The tropical tropopause layer
6 in reanalyses data sets, to be submitted to ACPD May 2019.
- 7 Tissier, A.-S. and Legras, B.: Convective sources of trajectories traversing the tropical
8 tropopause layer, *Atmos. Chem. Phys.*, 16, 3383–3398, doi:10.5194/acp-16-3383-2016, 2016.
- 9 Wales, P. A., Salawitch, R. J., Nicely, J. M. Anderson, D. C., Canty, T. P., Baidar, S., et al.,
10 Stratospheric injection of brominated very short-lived substances: Aircraft observations in the
11 Western Pacific and representation in global models. *Journal of Geophysical Research:*
12 *Atmospheres*, 123. [https://doi.org/ 10.1029/2017JD027978](https://doi.org/10.1029/2017JD027978), 2018.
- 13 Wang, B., J. Liu, H. J. Kim, P. J. Webster, and S. Y. Yim: Recent change of the global monsoon
14 precipitation (1979–2008), *Clim. Dyn.*, 39, 1123–1135, doi:10.1007/s00382-011-1266-z, 2012.
- 15 Warwick, N. J., J. A. Pyle, G. D. Carver, X. Yang, N. H. Savage, F. M. O'Connor, and R. A.
16 Cox: Global modeling of biogenic bromocarbons, *J. Geophys. Res.*, 111, D24305,
17 doi:10.1029/2006JD007264, 2006.
- 18 Wolter, K. and Timlin, M. S.: El Niño/Southern Oscillation behaviour since 1871 as diagnosed
19 in an extended multivariate ENSO index (MEI.ext). *Int. J. Climatol.*, 31: 1074-1087.
20 doi:10.1002/joc.2336, 2011.
- 21 Yamamoto, H., Yokouchi, Y., Otsuki, A., and Itoh, H.: Depth pro- files of volatile halogenated
22 hydrocarbons in seawater in the Bay of Bengal, *Chemosphere*, 45, 371–377,
23 doi:10.1016/s0045- 6535(00)00541-5, 2001.
- 24 Yang, X., Cox, R. A., Warwick, N. J., Pyle, J. A., Carver, G. D., O'Connor, F. M., and Savage,
25 N. H.: Tropospheric bromine chemistry and its impacts on ozone: A model study, *J. Geophys.*
26 *Res.*, 110, D23311, doi:10.1029/2005JD006244, 2005.
- 27 Yang, X., Pyle, J. A., Cox, R. A., Theys, N., and Van Roozendael, M.: Snow-sourced bromine
28 and its implications for polar tropospheric ozone, *Atmos. Chem. Phys.*, 10, 7763-7773,
29 doi:10.5194/acp-10-7763-2010, 2010.
- 30 Yang, X., Abraham, N. L., Archibald, A. T., Braesicke, P., Keeble, J., Telford, P. J., Warwick,
31 N. J., and Pyle, J. A.: How sensitive is the recovery of stratospheric ozone to changes in
32 concentrations of very short-lived bromocarbons?, *Atmos. Chem. Phys.*, 14, 10431-10438,
33 doi:10.5194/acp-14-10431-2014, 2014.
- 34 Ziska, F., Quack, B., Abrahamsson, K., Archer, S. D., Atlas, E., Bell, T., Butler, J. H.,
35 Carpenter, L. J., Jones, C. E., Harris, N. R. P., Hepach, H., et al.: Global sea-to-air flux



- 1 climatology for bromoform, dibromomethane and methyl iodide, Atmospheric Chemistry and
- 2 Physics Discussions, 13(2), 5601–5648, doi:10.5194/acpd-13-5601-2013, 2013.

- 3 Ziska, F., Quack, B., Tegtmeier, S., Stemmler, I., and Krüger, K.: Future emissions of marine
- 4 halogenated very-short lived substances under climate change. Journal of Atmospheric
- 5 Chemistry, 74: 245. <https://doi.org/10.1007/s10874-016-9355-3>, 2017.

- 6